

Synthesis and structure of SrCo_2Si_2 and CaRh_2Si_2 - isoelectronic variants of the parent superconductors AeFe_2As_2 and study of the influence of the valence electron count in $\text{CaFe}_{2-x}\text{Rh}_x\text{Si}_2$

Viktor Hlukhyy^{*}, Andrea V. Hoffmann, Thomas F. Fässler

Department Chemie, Technische Universität München, Lichtenbergstr. 4, D-85747 Garching, Germany

Received,

^{*} Corresponding author:

Dr. Viktor Hlukhyy, Department Chemie, Technische Universität München, Lichtenbergstr. 4, D-85747 Garching, Germany
E-mail: viktor.hlukhyy@lrz.tu-muenchen.de

Abstract

The finding of superconductivity in $\text{Ba}_{0.6}\text{K}_{0.4}\text{Fe}_2\text{As}_2$ put the attention on the investigation of compounds that crystallize with ThCr_2Si_2 structure type such as AT_2X_2 (A = alkali/ alkaline earth/ rare earth element; T = transition metal and X = element of the 13-15th group) . In this context the silicides CaFe_2Si_2 , $\text{CaFe}_{0.68(6)}\text{Rh}_{1.32(6)}\text{Si}_2$, CaRh_2Si_2 and SrCo_2Si_2 have been synthesized by melting mixtures of the elements in an arc-furnace under an argon atmosphere. Single crystals were obtained by special heat treatment in welded niobium ampoules. The compounds were investigated by means of powder and single crystal X-ray diffraction. All compounds crystallize in the ThCr_2Si_2 -type structure with space group $I4/mmm$ (No. 139): $a = 3.939(1) \text{ \AA}$, $c = 10.185(1) \text{ \AA}$, $R_1 = 0.045$, 85 F^2 values, 8 variable parameters for CaFe_2Si_2 ; $a = 4.0612(3) \text{ \AA}$, $c = 9.9373(9) \text{ \AA}$, $R_1 = 0.030$, 90 F^2 values, 10 variable parameters for $\text{CaFe}_{0.68(6)}\text{Rh}_{1.32(6)}\text{Si}_2$; $a = 4.0695(1) \text{ \AA}$, $c = 9.9841(3) \text{ \AA}$, $R_1 = 0.031$, 114 F^2 values, 8 variable parameters for CaRh_2Si_2 ; $a = 3.974(1) \text{ \AA}$, $c = 10.395(1) \text{ \AA}$, $R_1 = 0.036$, 95 F^2 values, 8 variable parameters for SrCo_2Si_2 . The structure of SrCo_2Si_2 contains isolated $[\text{Co}_2\text{Si}_2]^{2-}$ 2D-layers in the ab plane whereas in $\text{CaFe}_{2-x}\text{Rh}_x\text{Si}_2$ the $[\text{T}_2\text{Si}_2]$ layers ($T = \text{Fe}, \text{Rh}$) are interconnected along the c axis via Si-Si bonds resulting in a three-dimensional (3D) $[\text{T}_2\text{Si}_2]^{2-}$ and therefore belong to the so-called collapsed form of the ThCr_2Si_2 -type structure. The SrCo_2Si_2 and CaRh_2Si_2 are isoelectronic to the parent 122 iron-pnictide superconductors AeFe_2As_2 , whereas CaFe_2Si_2 is a full substituted variant (As/Si) of CaFe_2As_2 . The crystal chemistry and chemical bonding in the title compounds are discussed in terms of LMTO band structure calculations and a topological analysis using the Electron Localization Function (ELF).

Keywords: Alkaline earth metal, ThCr_2Si_2 -type structure, Superconductivity, Silicide, Chemical bonding

1. Introduction

The discovery of the superconducting behavior of $\text{Ba}_{0.6}\text{K}_{0.4}\text{Fe}_2\text{As}_2$ [1] renewed the interest in the ternary intermetallic compounds with the composition AT_2X_2 (A = alkali/alkaline earth/ rare earth element; T = transition metal and X = element of the 13-15th group). More than 600 compounds are already known that generally crystallize with the ThCr_2Si_2 structure type [2-4]. Interestingly the ternary parent compounds of the Fe-pnictide superconductors show no superconducting behavior but superconductivity emerges under external pressure or by chemical substitution [5]. Recently low temperature onset values (T_c) for the superconducting state at ambient pressure have been reported for some $A\text{Fe}_2X_2$ (A = K, Rb, Cs; X = As [6, 7], Se [8, 9]). In case of 122 iron selenides it was observed that the Fe-vacancies in the crystal lattice play a crucial role in the emergence of superconductivity. Generally, for the occurrence of superconducting behavior under ambient pressure the parent 122 compounds need some kind of substitution at one of the atom sites which can be categorized into electron-poor [1], electron-rich [10] or electron-equal substitution [11]. Due to the large variety of compounds with ThCr_2Si_2 -type structure they have high chemical flexibility and plenty of substitution possibilities are given. Recently attention was paid also to a series of the iron- and arsenic-free AeT_2X_2 phases (Ae = alkaline earth metal, T = Ni, Pd; X = P, Ge) with very low transition temperatures ($T_c \sim 0.3 - 3.0$ K) [12-15]. Undoped $RT_2\text{Si}_2$ (R = La, Y, Th; T = Ir, Pt) superconductors are also known, crystallizing however in CaBe_2Ge_2 -type structure [16]. Most of the known 122 transition metal silicides have rare earth metals at the A site. Compounds with alkaline earth metals at this site crystallizing in the ThCr_2Si_2 -type structure are limited [2, 3, 17-23].

In this work four new phases with alkaline earth metals on the A -site crystallizing in the ThCr_2Si_2 -type structure are presented. Moreover, CaFe_2Si_2 , CaRh_2Si_2 and SrCo_2Si_2 are the first ternary compounds in the respective $Ae/T/\text{Si}$ (Ae = Ca, Sr; T = Fe, Rh, Co) phase diagrams. CaFe_2Si_2 extends the row of CaT_2Si_2 compounds containing 3d-block transition metals (T = Co-Zn) [3, 18, 19, 21]. SrCo_2Si_2 represents the third ternary SrT_2Si_2 compound (T = 3d-block transition metals) besides SrCu_2Si_2 [23] and SrZn_2Si_2 [21]. For SrT_2Si_2 the isostructural compounds with T = Pd, Ag have been characterized and reported [20, 22]. CaRh_2Si_2 , the heavier homolog to the CaCo_2Si_2 [3], is only the second CaT_2Si_2 compound (T = 4d-block transition metals) besides CaPd_2Si_2 [20]. BaRh_2Si_2 [24] has been reported as well but the compound crystallizes in the BaIr_2Si_2 structure type.

One interesting feature for the AT_2X_2 compounds is the phenomenon of the lattice collapse. Depending on the distance between two $[T_2X_2]^{2-}$ layers, a possible covalent $X-X$ bond, which leads to the collapse of the structure, can be observed [25, 26]. The nature of the $X-X$ interactions importantly changes the structural parameters and has a significant influence on the electronic structure. The shape of the $[TX_4]$ tetrahedra and the distance separating the adjacent $[T_2X_2]^{2-}$ layers have also a great influence on the electronic states at the Fermi level. Since $SrCo_2Si_2$ and $CaRh_2Si_2$ are isoelectronic to the parent Fe-pnictide superconductors $AeFe_2As_2$, and $CaFe_2Si_2$ is full substituted variant of $CaFe_2As_2$ [27] at the X site, comparison of their electronic bonding situation will be of special interest.

2. Experimental Section

2.1. Syntheses

Starting materials for the syntheses of the title compounds were commercially available elements with high purity: ingots of calcium (Alfa Aesar, 99.5 %, redistilled prior to use), lumps of strontium (ChemPur, 98+ %, redistilled prior to use), rhodium shots (Alfa Aesar, 99.9+ %), iron granules (Alfa Aesar, 99.98 %) and silicon pieces (Alfa Aesar, 99.999 %). The sample preparations, arc-melting processes as well as the filling and sealing of the ampoules were performed in an argon-filled glovebox (MBraun 20 G, argon purity 99.996 %). Stoichiometric amounts of the transition metals cobalt, iron or rhodium and silicon (1:1) were pre-melted in an arc-furnace (Mini Arc Melting System, MAM-1, Johanna Otto GmbH).

For the synthesis of $CaFe_2Si_2$ 0.3 g ground FeSi powder was transferred to a niobium ampoule and the alkaline earth metal was added in the ratio 1:2 (Ca:"FeSi", overall mass of 0.372 g), afterwards the ampoule was sealed. The sample was heat-treated in a resistance furnace (HTM Reetz GmbH, Model LOBA 1200-40-600, connected to a thermo controller (EUROTHERM Deutschland GmbH). The ampoule was placed in an evacuated silica tube, heated to approximately 1223 K (Nabertherm, Controller P333) and held at this temperature for 24 h. Afterwards the temperature was reduced to approximately 1073 K in 25 h, kept at this temperature for 240 h and then cooled to room temperature within 4.5 h.

The $CaRh_2Si_2$ sample was prepared in an arc furnace by first pre-melting stoichiometric amounts of Rh and Si (1:1) and then adding Ca ingots in excess (1.5:2 Ca:"RhSi") to counteract the evaporation losses. The sample was afterward annealed in an induction furnace (Hüttinger Elektronik, Freiburg, Typ TIG 2.5/300 equipped with a Sensor

Therm Metis MS06 pyrometer for temperature monitoring) to improve homogeneity and single crystal quality. The sample was ground, pressed to a tablet and sealed in a tantalum ampoule. The ampoule was placed in a water-cooled sample chamber of an induction furnace, heated under a flow of argon to approximately 1273 K and held at this temperature for 1 h. The sample was cooled to room temperature within 2 h.

The quaternary compound $\text{CaFe}_{0.68(6)}\text{Rh}_{1.32(6)}\text{Si}_2$ was prepared by melting the elements in a stoichiometric composition of 1:1:1:2 (Ca:Rh:Fe:Si). The sample was heated in a welded Ta-ampoule to 1273 K for 12 h and then reducing the temperature to 1223 K holding it for 48 h in a resistance furnace. The sample was then ground and pelletized and annealed at 1423 K for 12 h followed by 100 h at 1323 K.

For the SrCo_2Si_2 compound (overall mass of 0.5 g) strontium was added to the “CoSi” pellet (Sr : “CoSi” ratio of 1 : 2) and melted three consecutive times in an arc-furnace to obtain higher homogeneity of the product. Single crystals were obtained from that sample. In addition a sample was synthesized in a niobium ampoule containing the pre-melted “CoSi” ground to a fine powder and stoichiometric amount of Sr (Sr : “CoSi” ratio of 1 : 2) and heat treated analog to the CaFe_2Si_2 sample.

The samples of SrCo_2Si_2 and CaFe_2Si_2 are not stable against air and moisture due to SrSi and Ca_5Si_3 impurities, respectively. Both Rh-containing samples are air stable. However, all reported intermetallic compounds are stable against air and moisture. Small single crystals of the three compounds could be isolated; they exhibited a plate-like crystal shape.

2.2. X-ray investigations

The purity of the SrCo_2Si_2 and CaRh_2Si_2 samples was checked at room temperature using a STOE Stadi P powder diffractometer with Cu- K_α radiation ($\lambda = 1.54056 \text{ \AA}$, Ge(111) monochromator). The iron containing samples were tested with a STOE Stadi P powder diffractometer with Mo- K_α radiation ($\lambda = 0.71070 \text{ \AA}$, Ge(111) monochromator). The powder X-ray diffraction pattern of the samples showed that all samples contained besides the ternary also known binary compounds as impurities. In case of SrCo_2Si_2 the additional phase was air sensitive SrSi and air stable CoSi, for CaFe_2Si_2 it was air sensitive Ca_5Si_3 and air stable FeSi, for CaRh_2Si_2 air stable RhSi was detected as a side phase and for $\text{CaFe}_{0.68(6)}\text{Rh}_{1.32(6)}\text{Si}_2$ air stable FeSi was observed. Attempts to synthesize purer samples have failed. The tetragonal lattice parameters for all three ternary title compounds (see Table 1) were obtained from

least-square fits of the powder X-ray diffraction data using WinXPOW [28]. The powder diffraction patterns are given in the Supporting Information, Figure S1-S4.

For the single crystal measurements the crystals were mounted on the tip of a glass fibre under a microscope using nail polish as glue. Single-crystal intensity data for SrCo_2Si_2 , CaRh_2Si_2 and $\text{CaFe}_{0.68(6)}\text{Rh}_{1.32(6)}\text{Si}_2$ were collected at room temperature using an Oxford Diffractions Xcalibur 3 diffractometer with graphite monochromatized Mo-K_α ($\lambda = 0.71071 \text{ \AA}$) radiation. Single-crystal data for the CaFe_2Si_2 compound was collected at room temperature using a Stoe IPDS-2T image plate diffractometer with graphite monochromatized Mo-K_α ($\lambda = 0.71071 \text{ \AA}$) radiation. The raw data were corrected for background, polarization and Lorentz factor. For SrCo_2Si_2 , CaRh_2Si_2 and $\text{CaFe}_{0.68(6)}\text{Rh}_{1.32(6)}\text{Si}_2$ an empirical absorption correction was applied [29] and for CaFe_2Si_2 a semi-empirical absorption correction was performed [30-32].

The starting atomic parameters were deduced from an automatic interpretation of direct methods with SHELXS-97 [33]. For the subsequent refinement for the ternary compounds the lattice parameters determined from the X-ray powder diffraction measurements were given as input data. In case of $\text{CaFe}_{0.68(6)}\text{Rh}_{1.32(6)}\text{Si}_2$ the lattice parameters from single crystal X-ray diffraction measurement were used. The structures were then refined using SHELXL-97 (full-matrix least-square on F_o^2) [34] with anisotropic atomic displacement parameters for all atoms. The occupancy parameters for each atom were refined in separate least-squares cycles to check the correct composition of the compounds. The refinements showed that all atom sites in CaFe_2Si_2 , CaRh_2Si_2 and SrCo_2Si_2 are fully occupied, whereas in $\text{CaFe}_{0.68(6)}\text{Rh}_{1.32(6)}\text{Si}_2$ the transition metal site was occupied to 66(3) % with Rh and to 34(3) % with Fe. No significant residual peaks were observed for a difference electron-density (Fourier) synthesis. The interatomic distances given in the article refer to the single crystal diffraction data of SrCo_2Si_2 , CaFe_2Si_2 and CaRh_2Si_2 using the lattice parameters determined by X-ray powder diffraction as input for the structure refinement. The relevant crystallographic data for the data collection and the structure refinement are listed in Table 1. Further details of the structure determinations may be obtained from: Fachinformationszentrum Karlsruhe, D-76344 Eggenstein-Leopoldshafen, Germany (fax: +49-7247-808-666; email: crysdata@fiz-karlsruhe.de) by quoting the Registry No's. CSD-425467 (CaFe_2Si_2), -425468 ($\text{CaFe}_{0.68(6)}\text{Rh}_{1.32(6)}\text{Si}_2$), -425469 (CaRh_2Si_2), and -425470 (SrCo_2Si_2).

After data collection the single crystals were analyzed by EDX measurements using a JEOL SEM 5900 LV Scanning Electron Microscope equipped with an Oxford Instruments

INCA energy dispersive X-ray microanalysis system. The semi-quantitative EDX analysis reveals the elemental compositions (values given in at. %): Sr 24(3), Co 38(5) and Si 38(5) for SrCo_2Si_2 ; Ca 21(2), Fe 42(4) and Si 38(3) for CaFe_2Si_2 ; Ca 20(2), Rh 42(4) and Si 38(4) for CaRh_2Si_2 ; Ca 19(2), Fe 12(2), Rh 30(4) and Si 39(4) for $\text{CaFe}_{0.68(6)}\text{Rh}_{1.32(6)}\text{Si}_2$, which within standard deviations corresponds to the compositions of the title phases.

2.3. *Magnetic measurements*

Magnetic measurements were performed using a MPMS XL5 SQUID magnetometer (Quantum Design). All samples were investigated with a zero-field cooled / field-cooled (zfc-fc) measurement and magnetization measurement. The temperature range for the zfc-fc measurements was between 1.8 and 30 K (1.8-15 K for the CaRh_2Si_2 sample), for the field-cooled part a field (H) of $1.5 \cdot 10^{-4}$ T was applied. The magnetic behaviour was measured at room temperature up to 5 T. All data were corrected for the holder and for the diamagnetic contribution of the core electrons.

None of the title compounds show superconductive behavior down to 1.8 K. Due to ferromagnetic impurities the samples of SrCo_2Si_2 , CaFe_2Si_2 and $\text{CaFe}_{0.68(6)}\text{Rh}_{1.32(6)}\text{Si}_2$ showed ferromagnetic behaviour in the measured field range. The CaRh_2Si_2 sample showed diamagnetic behaviour for fields higher than 0.5 T, whereas in the measured range between 0.01-0.5 T the magnetization has a positive value indicating paramagnetic influences for CaRh_2Si_2 .

2.4. *Electronic structure calculations*

The electronic structures for the ternary title compounds were calculated employing a linear muffin-tin orbital (LMTO) method in the atomic sphere approximation (ASA) in the tight-binding (TB) program [35]. The radii of the muffin-tin spheres and empty spheres were determined after Jepsen and Andersen [36]. The Brillouin zone integrations were performed with a $16 \times 16 \times 32$ special k -point grid. The basis set of short-ranged [37] atom-centered TB-LMTOs contained s , d valence functions for Ca and Sr; s - d valence functions for Fe, Co, and Rh; s , p valence functions for Si. Ca $4p$ and Sr $5p$ orbitals were included using a downfolding technique.

The analysis of the chemical bonding is based upon theoretical partial and total density of states (DOS) curves, plots of the crystal orbital Hamilton populations (COHPs) [38], band structures with fatbands and contour line diagrams of the Electron Localization Function

(ELF) [39]. From the COHP analyses the contribution of the covalent part of a particular interaction to the total bonding energy of the crystal can be obtained. The atomic orbital character is represented as a function of the band width in the fatband analysis.

3. Results and Discussions

The four title compounds CaFe_2Si_2 , $\text{CaFe}_{0.68(6)}\text{Rh}_{1.32(6)}\text{Si}_2$, CaRh_2Si_2 and SrCo_2Si_2 , adopt the ThCr_2Si_2 -type structure (Figures 1). The ThCr_2Si_2 -type structure has been described in detail before [25, 40]. Main motifs of this structure are the $\infty^2[T_2X_2]^{2-}$ layers which contain $[TX_4]$ edge shared tetrahedra in the ab plane. The T atoms form a square-planar arrangement in the ab plane and are tetrahedrally coordinated by Si atoms that are situated in analogy to a chess board alternating above and below the squares of T atoms. The distortion from tetrahedral symmetry is influenced by the T - T , T - X interactions in the layers and X - X interactions between the layers. The tunable distance between the X atoms of adjacent layers is an important factor in this structure type which determines if the $[T_2X_2]^{2-}$ layers are restricted in the ab plane (two-dimensional) or build a 3D (three-dimensional) network. The layers are separated by cations which are located in the cavities created by eight tetrahedra of two adjacent layers. The structure of SrCo_2Si_2 contains isolated $[\text{Co}_2\text{Si}_2]^{2-}$ 2D-layers in the ab plane, whereas the $[T\text{-Si}]$ layers ($T = \text{Fe, Rh}$) in $\text{CaFe}_{2-x}\text{Rh}_x\text{Si}_2$ are interconnected along the c axis via Si-Si bonds resulting in a $[T_2\text{Si}_2]^{2-}$ 3D-network.

Table 5 lists some structural parameters for different AeT_2Si_2 ($\text{Ae} = \text{Ca-Ba}$, $T = \text{Fe-Zn, Pd, Ag, Rh}$) [2, 3, 20-23, 41] compounds including the data for the ternary title compounds. In addition the structural parameters for the AeT_2Ge_2 ($\text{Ae} = \text{Ca-Ba}$, $T = \text{Mn-Zn}$) [17, 23] compounds are given in Table S1 (Supporting information).

3.1. Crystal structure of CaFe_2Si_2

CaFe_2Si_2 is the first reported compound in the AeFe_2X_2 systems ($\text{Ae} = \text{alkaline-earth metal}$, $X = \text{group 14 elements}$). Although the parent compounds of the iron pnictides superconductors AeFe_2Pn_2 have been studied extensively, the analogue tetrelides have not been investigated so far. The substitution of Co in CaFe_2Si_2 does almost not influence the lattice parameter a (3.939(1) Å for CaFe_2Si_2 and 3.92 Å for CaCo_2Si_2 [3]) and the interatomic distances d_{T-T} in the $[T_2X_2]^{2-}$ layers are very similar (2.785(1) Å and 2.77 Å for CaFe_2Si_2 and CaCo_2Si_2 , respectively). However it has a significant impact on the lattice parameter c , heights of Si atoms above T layer, the distances $d_{T\text{-Si}}$, $d_{\text{Si-Si}}$ and the tetrahedral angle α . The c

parameter is almost 0.2 Å longer in the Fe-compound (10.185(1) Å vs 9.92 Å for CaCo₂Si₂) and correspondingly the volume of the unit cell decreases from 158.0(1) Å³ in CaFe₂Si₂ to 152.1 Å³ for CaCo₂Si₂. The $[T_2X_2]^{2-}$ layers are further apart due to the increase of the c parameter. The heights of Si atoms above T layer are 1.269 Å for CaFe₂Si₂ and 1.190 Å for CaCo₂Si₂, which is also reflected in the interlayer $d_{\text{Si-Si}}$ (2.555(9) Å in CaFe₂Si₂ and 2.58 Å in CaCo₂Si₂). Hoffmann and Zheng have observed the trend that the d_{X-X} values should decrease for a system AeT_2X_2 (same Ae and X) when moving from the left-hand side of the periodic table to the right-hand side for the T element [26]. They placed their observation on ternary compounds where $T = P$. The P-containing compounds belong to the compounds with uncollapsed ThCr₂Si₂ type structure for transition metals on the left-hand side of the periodic table. In the case of CaFe₂Si₂ and CaCo₂Si₂ a differentiation of this trend is observed since the Fe-compound has the shorter $d_{\text{Si-Si}}$ value. Comparing the ThT₂Si₂ ($T = \text{Cr-Cu}$) crystallographic data a similar effect can be seen when comparing the ThCo₂Si₂ compound with the ThFe₂Si₂ compound [42]. It seems that the trend of decreasing d_{X-X} interactions for AT_2X_2 compounds (A = alkaline earth metals or rare earth metals, X = tetrels), when moving to the left-hand side of the Periodic Table (for $T = \text{Mn-Zn}$), is not a uniform trend for compounds with collapsed ThCr₂Si₂ structure type.

The geometry of the tetrahedra in $[T_2Si_2]^{2-}$ changes as a result of the different height of Si atoms above T layer. In CaFe₂Si₂ the $d_{\text{Fe-Si}}$ value is slightly elongated (2.343(2) Å) compared to $d_{\text{Co-Si}}$ of 2.29 Å in CaCo₂Si₂ and the α values decreases (114.4(2) ° for CaCo₂Si₂ and 117.4 ° for CaCo₂Si₂).

It should be mentioned that the structure of the well-known superconductor compound CaFe₂As₂ [27], where Si is fully substituted (Si/As), contains no $X-X$ interlayer bonds at ambient pressure whereas in the high-pressure modification this covalent bonds emerges [43, 44]. CaFe₂As₂ has a slightly shorter lattice parameter a of 3.87 Å than the CaFe₂Si₂ compound (3.939(1) Å), indicating stronger Fe-Fe interactions (d_{T-T} of 2.74 Å for CaFe₂As₂ and 2.785(1) Å for CaFe₂Si₂). The values of the lattice parameters c and V differ noticeably ($c = 11.73$ Å, $V = 175.94$ Å³ for ucT-CaFe₂As₂ at ambient pressure) [27]. The discrepancy is due to the non-existing As-As bonds along the c direction. The height of As atoms above Fe-layer is influenced by the missing As-As bonds (1.367 Å for CaFe₂As₂ and 1.269 Å for CaFe₂Si₂). The Si-Si-bond in CaFe₂Si₂ results in a vertical displacement of the Si atomic z -coordinate towards higher values to accommodate the covalent bond compared to the 2-D layered structure of CaFe₂As₂. The tetrahedral angle α is close to the ideal tetrahedral angle of

109.4 ° in ucT-CaFe₂As₂ (109.5 °) but is larger in CaFe₂Si₂ (114.4(2) °), which is in accordance with the structural properties of other reported 122 arsenides and silicides [3].

3.2. Crystal structure of CaRh₂Si₂

CaRh₂Si₂ is isoelectronic to CaFe₂As₂ and is analogue to CaCo₂Si₂ [3] with the heavier homologue on the transition metal position. The increased covalent radius of Rh (1.350 Å to 1.240 Å for Co) [33, 34] mainly affects the parameters and distances connected to the square transition metal plane in the *ab* plane. The lattice parameter *a* is 0.15 Å larger for CaRh₂Si₂ (4.070(1) Å) compared to CaCo₂Si₂ (3.92 Å) resulting in an elongation of the distances between the transition metal atoms (2.878(1) Å and 2.77 Å, respectively) and the Si atoms in that plane.

The values for the *c* parameter vary less (9.984(1) Å and 9.92 Å respectively) and so should the distance between the [T₂X₂]²⁻ layers. The heights of Si atoms above *T* layer is larger in the CaRh₂Si₂ (1.231 Å) than in CaCo₂Si₂ (1.190 Å). The distance between the interlayer Si-Si atoms is shorter (*d*_{Si-Si} = 2.529(8) Å for CaRh₂Si₂ and 2.58 Å for CaCo₂Si₂) resulting in stronger Si-Si interactions. Due to the longer *T-T* distance for the Rh-compound and the larger height of Si atoms the *T-Si* distance has to increase (2.378(1) Å for CaRh₂Si₂ and 2.29 Å for CaCo₂Si₂). Those changes result in almost unchanged tetrahedral angle in the [T₂X₂]²⁻ layers (117.6(3) ° for CaRh₂Si₂ and 117.4 ° for CaCo₂Si₂). Similar observations can be made for the comparison between AeNi₂Si₂ and AePd₂Si₂, containing transition metal homologues (see Table 5).

3.3. Crystal structure of CaFe_{0.68(6)}Rh_{1.32(6)}Si₂

The values of the *a* lattice parameter, volume, *T-T* and *T-Si* interatomic distances of quaternary compound CaFe_{0.68(6)}Rh_{1.32(6)}Si₂ are between those of the side compounds CaFe₂Si₂ and CaRh₂Si₂ but closer to those of CaRh₂Si₂ due to the higher Rh-content, approaching Vegard's law (Tables 1 and 3). However, an anomalous compression of the *c* parameter of CaFe_{0.68(6)}Rh_{1.32(6)}Si₂ in comparison to the side ternary compounds is observed. In order to maintain the interlayer Si-Si distance almost the same as in CaFe₂Si₂ (with largest *c*) the height of Si atoms above *T* layer is smaller and the tetrahedral angle α is flattened.

This is in contrast to the CaFe_{2-x}Rh_xAs₂ solid solution for which nearly linear variety in the lattice parameters was reported, however, only for the region of *x* = 0 - 0.6 [45]. Nevertheless, when comparing the lattice parameters with those of CaRh₂As₂ [46] the

deviation from linearity becomes noticeable. Therefore further studies of the T/T substitution in AeT_2X_2 phases are required for better understanding of the structural properties in these systems.

3.4. Crystal structure of $SrCo_2Si_2$

$SrCo_2Si_2$ has the smallest lattice parameter a and volume ($a = 3.974(1) \text{ \AA}$, $V = 164.2(1) \text{ \AA}^3$) compared to $SrCu_2Si_2$ and $SrZn_2Si_2$ (4.20 \AA and 4.33 \AA , 179.4 \AA^3 and 194.1 \AA^3 , respectively), but the largest c parameter ($10.395(2) \text{ \AA}$, 10.00 \AA and 10.35 \AA , respectively) [21, 23]. To account for this effect the interaction in the ab plane has to be stronger for $SrCo_2Si_2$ but are weakened along the c axis, which is reflected in the $T-T$, $T-Si$ and $Si-Si$ interatomic distances. The elongation of the c axis is a result of the different bonding situation between the adjacent tetrahedral-layers. In $SrCu_2Si_2$ the $[T_2X_2]^{2-}$ layers are connected via $Si-Si$ covalent bonds (2.42 \AA) resulting in the collapsed $ThCr_2Si_2$ type structure, whereas in $SrCo_2Si_2$ the $Si-Si$ distance is elongated ($2.898(5) \text{ \AA}$) which indicates that the layers are well separated without covalent bonds in between. This observation is in accordance with the results published by Hoffmann and Zheng [26], stating that d_{X-X} decreases as the transition metal T moves from the left-hand side to the right-hand side in the Periodic Table. At this point the SrT_2Si_2 and SrT_2Ge_2 systems ($T = Mn-Zn$) show a deviation (Table 5; Supporting information, Table S1). Even though the d_{Ge-Ge} decreases when going from Co ($d_{Ge-Ge} = 2.90 \text{ \AA}$) to Ni ($d_{Ge-Ge} = 2.83 \text{ \AA}$) they are certainly longer than that of a $Ge-Ge$ covalent single bond in diamond-like Ge (2.45 \AA). Only the $SrMn_2Ge_2$ ($d_{Ge-Ge} = 2.63 \text{ \AA}$), possibly $SrCu_2Ge_2$ ($d_{Ge-Ge} = 2.70 \text{ \AA}$) and definitely $SrZn_2Ge_2$ ($d_{Ge-Ge} = 2.50 \text{ \AA}$) can be considered as having a covalent interlayer $Ge-Ge$ bond. Since the $X-X$ interactions are weakened the $T-T$ and $T-X$ interactions in the $[T_2X_2]^{2-}$ layer are more prominent as can be seen from the corresponding values in Tables 5 and S1 (Supporting information). For $SrCo_2Si_2$ the $T-T$ and $T-Si$ distances in the $[T_2Si_2]^{2-}$ layers are shorter than for $SrCu_2Si_2$ ($2.810(1) \text{ \AA}$ and $2.296(3) \text{ \AA}$ compared to 2.97 \AA and 2.47 \AA , respectively).

Due to the shorter distances in the $[T_2Si_2]^{2-}$ layer and the smaller height of Si atoms above T layer (1.150 \AA for $SrCo_2Si_2$ and 1.290 \AA for $SrCu_2Si_2$ [23]) the tetrahedra are flattened in $SrCo_2Si_2$ resulting in a larger tetrahedra angle α compared to $SrCu_2Si_2$ ($119.1(2)^\circ$ to 116.9°). The influence of the deformation of the $[TX_4]$ tetrahedra from an ideal tetrahedron $\alpha = 109.4^\circ$ has been already discussed for the CaT_2Ge_2 compounds [21]. By varying the transition metal from Mn to Zn the tetrahedral angle increases from 111.3° for Mn to 119.1°

for Ni and then decreases to 114.9 ° for Cu and 109.9 ° for Zn (Supporting information, Table S1). The almost ideal tetrahedral structure for CaZn_2Ge_2 can be attributed to the filled 3d-shell. Unfortunately, it is impossible to detect a trend for the SrT_2Si_2 compounds since only crystallographic data for $T = \text{Co}, \text{Cu}$ is available.

When comparing SrCo_2Si_2 with CaCo_2Si_2 the expected differences in the parameters are observed. First of all are the lattice parameters (a and c parameter and correspondingly V) all larger for the Sr-compound due to the large ionic radius of Sr^{2+} (1.18 Å compared to 1.00 Å for Ca^{2+}) [47] as are the $d_{\text{Si-Si}}$ values (2.898(5) Å for SrCo_2Si_2 and 2.58 Å for CaCo_2Si_2) [3]. The heights of Si atoms above Co layer are smaller in SrCo_2Si_2 compared to CaCo_2Si_2 (1.150 Å and 1.190 Å, respectively). The CaCo_2Si_2 compound contains covalent Si-Si bonds along the c direction and belongs to the group of compounds with collapsed ThCr_2Si_2 -type structure. Analogous observations can be made for the corresponding Ge-compounds (Supporting information, Table S1). The value for $d_{\text{T-Si}}$ is very similar (2.29 Å in CaCo_2Si_2 and 2.296(3) Å in SrCo_2Si_2) but the $d_{\text{T-T}}$ value differentiates slightly (2.77 Å in CaCo_2Si_2 and 2.810(1) Å in SrCo_2Si_2), which in combination with the lattice parameter and the value of height of Si atoms leads to the higher α value of tetrahedral angle in SrCo_2Si_2 (119.9(2) ° vs 117.4 ° in CaCo_2Si_2). It is necessary to note, that the SrCo_2Si_2 is isoelectronic to the parent 122 iron-pnictide superconductors AeFe_2As_2 .

3.5. Electronic structure calculations

In the title silicides CaFe_2Si_2 , CaRh_2Si_2 and SrCo_2Si_2 , similar to other AeT_2X_2 phases, the bonding between Ae^{2+} and the $[\text{T}_2\text{X}_2]^{2-}$ layer is mainly ionic, while in the $[\text{T}_2\text{X}_2]^{2-}$ layers the covalent T - X bonds as well as weak metal-metal T - T bonds occur. In order to analyse the electronic properties of these compounds the total Density Of States (DOS) as well as the partial DOS were calculated (Figure 2).

Comparison of the DOS profiles for isostructural CaFe_2Si_2 , CaRh_2Si_2 and SrCo_2Si_2 allows us to understand the main differences of their electronic structure. No band gap is observed at the Fermi level in all cases indicating metallic properties of the title compounds. The DOS can be divided into two parts separated by a gap: one block at lower energies (from -10.5 to -6.5 eV for CaFe_2Si_2 , from -11 to -7.5 eV for CaRh_2Si_2 and from -11 to -7 eV for SrCo_2Si_2) and one from about -5.5 eV (CaFe_2Si_2), -6.5 eV (CaRh_2Si_2) and -5.5 eV (SrCo_2Si_2) up to energies above the Fermi level. The Si-s states are located at the bottom of the valence band (first block). The first half of the second block (from -5 to -1 eV for

CaFe₂Si₂, from -6.5 to -3.5 eV for CaRh₂Si₂ and from -5.5 to -2 eV for SrCo₂Si₂) is mainly build up from *T*-d and Si-p partial DOS of similar shape, indicating the hybridisation of these orbitals and correspondingly covalent *T*-Si bonds within $[T_2X_2]^{2-}$ layers. Calculation of the Crystal Overlap Hamiltonian Population (COHP) for this part of the DOS reveals good *T*-Si interactions (Table 3, Supporting Information, Figures S5-7). The upper half of the second block (from -1 eV for CaFe₂Si₂, -3.5 eV for CaRh₂Si₂ and -2 eV for SrCo₂Si₂ to E_F) is dominated by the *T*-d orbitals. It is well established that the electronic bands around the Fermi level are responsible for superconductivity. These bands are formed mainly by the d-states of the *T* atoms for CaFe₂Si₂ and, to a lesser effect, for SrCo₂Si₂ whereas the pseudogap is now situated at E_F for CaRh₂Si₂ with smaller *T*-d state contributions. The contributions of Ca/Sr states to the valence bands are negligible since these atoms are in the form of cations Ae^{2+} in the AeT_2X_2 structures and serve as electron-donors. The contribution of the Si atoms to the Fermi surface is small but non-zero.

The density of states of the examined silicides, going from CaFe₂Si₂ to CaRh₂Si₂ and SrCo₂Si₂, clearly shows a shifting of the Fermi level to conduction band in accordance with increasing of electron count. A local maximum at the Fermi level in CaFe₂Si₂, formed predominantly by Fe-d states, can be correlated to a degree of structural or magnetic instability observed in Fe-containing 122 superconductors. The rhodium silicide CaRh₂Si₂ has an increased valence electron count ($+2e$) as compared to CaFe₂Si₂, resulting in a shift of E_F from the local maximum DOS in CaFe₂Si₂ to a pseudogap between two local maxima in CaRh₂Si₂. Similar trend is observed for homologue CaCo₂Si₂ [3] (Supporting information, Figure S8), where the pseudogap is observed near the Fermi level. From CaRh₂Si₂ to SrCo₂Si₂ further shifting of E_F followed by the lowering of band dispersion are observed. Despite the same electron count in CaRh₂Si₂ and SrCo₂Si₂, the bonding situation in these structures seems to be different. The non-bonded Si atoms ($d_{Si-Si} = 2.898(5)$ Å) in SrCo₂Si₂ have the formal electron count $(2 \times Si)^{8-}$, whereas the singly bonded Si-Si dimer in CaRh₂Si₂ has a formal count of electrons $(Si-Si)^{6-}$, like the two non-bonded $(2 \times As)^{6-}$ in uncollapsed-tetragonal (ucT) Sr(Ba)Rh₂As₂ [48, 49]. This in turn affects the electron configuration of transition metal *T* atoms, taking into account that the charge of the cations Ae remains the same, and results in the shift of DOS near Fermi level. In this regard, the collapsed tetragonal (cT) CaFe₂Si₂ with $(Si-Si)^{6-}$ dimer is electronically close to the uncollapsed-tetragonal (ucT) CaFe₂As₂ with non-bonded $(2 \times As)^{6-}$, having similar formal charge distributions: $Ca^{2+}(Fe^{2+})_2(Si-Si)^{6-}$ vs $Ca^{2+}(Fe^{2+})_2(As^{3-})_2$. This is reflected in the similarities of the corresponding DOS: for

CaFe₂As₂ a similarly shaped density of states of Fe *d* bands near E_F and a pseudogap have also been observed [50].

The situation of the near E_F region in the DOS of the examined silicides is mirrored in the fatband analyses (Figures S9-S11, Supporting information). The contribution of the Fe $3d_{x^2-y^2}^2$ (pointing directly towards the nearest neighbor Fe atoms) and $3d_{xz,yz}$ orbitals is largest close to E_F for CaFe₂Si₂, which is indicated by the sharp peaks in the density of states. These orbitals are moved to lower energies in CaRh₂Si₂ and SrCo₂Si₂. The conduction band of the studied compounds has mainly $T-d_{xy}$ character, which lies near to E_F in SrCo₂Si₂, indicated by the sharp peak in DOS. The $T-d_{xz,yz}$ orbitals, pointing directly toward Si atoms, show strong hybridization in their lower part of energy with Si-*p* orbitals, indicating strong covalent *T*-Si bonding. However, several Si-*p* bands cross E_F in the mixing with *T-d* orbitals. In CaFe₂Si₂ the Si-*p* with Fe- d_z^2 bands cross E_F mostly in the section $Z \rightarrow \Gamma$ (crystallographic *c* direction), whereas in CaRh₂Si₂ the Si-*p* orbitals crossing E_F are hybridized along $Z \rightarrow \Gamma$ with Rh- d_z^2, xz, yz and along $\Gamma \rightarrow X$, $P \rightarrow N$ (crystallographic *ab*-plane) with Rh- $d_{xz,yz}$ orbitals. In SrCo₂Si₂ the Si-*p* bands that cross E_F are hybridized with Co- d_z^2 along $Z \rightarrow \Gamma$ and with Co- $d_{xz,yz,x^2-y^2}^2$ along $\Gamma \rightarrow X$, $P \rightarrow N$. This underlines the influence of *T*-Si bonding interactions on the Fermi surface.

Further insight in the nature of the bonding situation can be provided analysing the electron density in real space using the Electron Localization Function (ELF), sketched in Figure 3. The ELF reveals clearly a bisynaptic valence basin (> 0.72) between the Si atoms for the CaFe₂Si₂ and CaRh₂Si₂ structures. The basins are orientated towards each other indicating a localized covalent bond. Similar interlayer *X-X* bonds have been described in CaCo₂Si₂ and CaNi₂Ge₂ [3, 51]. Due to the longer Si-Si distance the ELF reveals no bisynaptic valence basin for SrCo₂Si₂ but non-bonding (monotactic) ELF domains (free electron pairs) which are located at the Si atoms with their orientation towards each other. These pairs are arranged closely and touch each other, indicating only very weak bonding interactions between the Si atoms (iCOHP value of 0.93 eV). In CaFe₂Si₂, CaRh₂Si₂, and SrCo₂Si₂ the ELF attractors at low values (0.39, 0.29 and 0.39, respectively) were observed between *T* atoms, forming a planar square net indicating directed bonding interactions. This is in agreement with results obtained for LaT₂Ge₂ (*T* = Mn, Fe, Co) [52].

4. Conclusions

The title intermetallic compounds CaFe₂Si₂, CaFe_{0.68(6)}Rh_{1.32(6)}Si₂, CaRh₂Si₂ and SrCo₂Si₂ crystallise in the ThCr₂Si₂-type structure and show the tunable Si-Si distance.

CaFe₂Si₂, CaRh₂Si₂ and SrCo₂Si₂ are the first ternary compounds in the respective *Ae/T/Si* (*Ae* = Ca, Sr; *T* = Fe, Rh, Co) phase diagrams. The anionic substructure in CaFe_{2-x}Rh_xSi₂ (*x* = 0, 1.32, 2) is best described as a three-dimensional ³_∞[T₂Si₂]²⁻ network with covalent Si-Si bonds between ²_∞[T₂Si₂]²⁻ layers and distances almost independent of *T* (2.529(8) - 2.555(9) Å). SrCo₂Si₂ consists of discrete two-dimensional ²_∞[Co₂Si₂]²⁻ layers (*d*_{Si-Si} = 2.898(5) Å). The comparison with other *AeT₂Si₂* compounds (*T* = Co-Zn) reveals that the change of the transition metal from the left-hand side to the right-hand side in the Periodic Table doesn't induce a linear decrease of the *X-X* distance, as was observed for the isostructural phosphides [26]. Analogously, no linear changes of geometrical parameters can be observed during the Fe/Rh substitution in CaFe_{2-x}Rh_xAs₂ solid solution. This can be explained by complex interplay between covalent, metallic and ionic interactions in ThCr₂Si₂-type compounds. The major contribution to the structural changes traces back to the size of the alkaline earth metal. The variation from the smaller calcium atom to the larger homologues strontium or barium in *AeT₂X₂* structures induces not only an increase of the *T-T* and *X-X* distances but also a flattening of the tetrahedral angle *X-T-X* (Table 5, S1). Interestingly, the series of electron richer compounds *RFe₂Si₂*, *RRh₂Si₂* and *RCo₂Si₂* (*R* – rare-earth metal) [3] are known with *R*³⁺ cations in the cavities of [T₂Si₂]³⁻ network, underlying the high chemical and electronic flexibility of ThCr₂Si₂-type structure. The results of the quantum chemical calculations concerning DOS, COHP and the band structures including fatbands have been discussed. The topological analysis of the ELF depicts clearly the Si-Si bond in CaFe₂Si₂ and CaRh₂Si₂ and the non-bonding Si-Si in SrCo₂Si₂, as well as weak directed bonding interactions between the transition metal atoms.

Acknowledgments

This research was supported by the Deutsche Forschungsgemeinschaft (Priority Program 1458).

Appendix A. Supplementary Information

Supplementary data associated with this article can be found in the online version at...

References

- [1] M. Rotter, M. Tegel, D. Johrendt, *Phys. Rev. Lett.* 101 (2008) 107006.
- [2] N. Nasir, N. Melnychenko-Koblyuk, A. Grytsiv, P. Rogl, G. Giester, J. Wosik, G.E. Nauer, *J. Solid State Chem.* 183 (2010) 565-574.
- [3] L. Siggelkow, V. Hlukhyy, T. Faessler, *Z. Anorg. Allg. Chem.* 636 (2010) 378-384.
- [4] G. Just, P. Paufler, *J. Alloy. Compd.* 232 (1996) 1-25.
- [5] N. Takeshita, R. Kobayashi, H. Fukazawa, Y. Kohori, K. Kihou, C.-H. Lee, H. Kito, A. Iyo, H. Eisaki, *Phys. Rev. B.* 81 (2010) 224511.
- [6] K. Sasmal, B. Lv, B. Lorenz, A.M. Guloy, F. Chen, Y.-Y. Xue, C.-W. Chu, *Phys. Rev. Lett.* 101 (2008) 107007.
- [7] H. Chen, Y. Ren, Y. Qiu, W. Bao, R.H. Liu, G. Wu, T. Wu, Y.L. Xie, X.F. Wang, Q. Huang, X.H. Chen, *EPL* 85 (2009) 17006.
- [8] A.L. Ivanovskii, *J. Phys. C* 471 (2011) 409-427.
- [9] J. Guo, S. Jin, G. Wang, S. Wang, K. Zhu, T. Zhou, M. He, X. Chen, *Phys. Rev. B.* 82 (2010) 180520.
- [10] A. Leithe-Jasper, W. Schnelle, C. Geibel, H. Rosner, *Phys. Rev. Lett.* 101 (2008) 207004.
- [11] Q. Tao, S. Jiang, C. Feng, C. Wang, J. Dai, G. Cao, Z.a. Xu, *Phys. Rev. Lett.* 102 (2009) 137002.
- [12] T. Mine, H. Yanagi, T. Kamiya, Y. Kamihara, M. Hirano, H. Hosono, *Solid State Commn.* 147 (2008) 111.
- [13] C.D. Yang, H.C. Hsu, W.Y. Tseng, H.C. Chen, H.C. Ku, M.N. Ou, Y.Y. Chen, Y.Y. Hsu, *J. Phys.: Conf. Ser.* 273 (2011) 012089.
- [14] F. Ronning, E.D. Bauer, T. Park, S.-H. Baek, H. Sakai, J.D. Thompson, *Phys. Rev. B.* 79 (2009) 134507.
- [15] H. Fujii, A. Sato, *Phys. Rev. B.* 79 (2009) 5.
- [16] R.N. Shelton, H.F. Braun, E. Musick, *Solid State Commn.* 52 (1984) 797-799.
- [17] W. Doerrscheidt, N. Niess, H. Schaefer, *Z. Naturforsch.* 31 (1976) 890-891.
- [18] W. Rieger, E. Parthé, *Monatsh. Chem* 100 (1969) 444.
- [19] O.I. Bodak, E.I. Gladyshevskii, *Dopov. Akad. Nauk Ukr. RSR* 30 (1968) 944.
- [20] A. Palenzona, S. Cirafici, F. Canepa, *J. Less Comm. Met.* 135 (1987) 185-194.
- [21] C. Kranenberg, D. Johrendt, A. Mewis, R. Pottgen, G. Kotzyba, H. Trill, B.D. Mosel, *J. Solid State Chem.* 167 (2002) 107-112.
- [22] N. May, H. Schaefer, *Z. Naturforsch.* 27 (1972) 864-865.
- [23] B. Eisenmann, N. May, W. Mueller, H. Schaefer, A. Weiss, J. Winter, G. Ziegler, *Z. Naturforsch.* 25 (1970) 1350-1352.
- [24] D. Langen, S. Schoolaert, H. Ploss, W. Jung, *Z. Anorg. Allg. Chem.* 623 (1997) 1561-1566.
- [25] G. Venturini, B. Malaman, *J. Alloy. Compd.* 235 (1996) 201-209.
- [26] R. Hoffmann, C. Zheng, *J. Phys. Chem.* 89 (1985) 4175-4181.
- [27] G. Wu, H. Chen, T. Wu, Y.L. Xie, Y.J. Yan, R.H. Liu, X.F. Wang, J.J. Ying, Chen, X.H., *J. Phys.: Condens. Matter* 20 (2008) 422201.
- [28] Stoe, WinXPOW Version 2.08 Stoe & Cie GmbH, Darmstadt 2003.
- [29] CrysAlis RED, Scale3 / ABSPACK, Version 1.171.33.34d Oxford Diffraction, Poland Sp. z o.o., 2009.
- [30] X-Area, MainMenu Version 1.26 STOE & Cie GmbH, Darmstadt (Germany) 2004.
- [31] X-RED32, Data Reduction Program, Version 1.48 STOE & Cie GmbH, Darmstadt (Germany) 2008.

- [32] X-SHAPE, Crystal Optimization for Numerical Absorption Correction, Version 2.11 STOE & Cie GmbH, Darmstadt (Germany) 2008.
- [33] G.M. Sheldrick, SHELXS-97, -Program for the Determination of Crystal Structures University of Goettingen (Germany) 1997.
- [34] G.M. Sheldrick, SHELXL-97, -Program for Crystal Structure Refinement University of Goettingen (Germany) 1997.
- [35] M.v. Schilfgarde, T.A. Paxton, O. Jepsen, O.K. Andersen, G. Krier, The Stuttgart Tight-Binding LMTO-ASA program Version 4.7 Max Planck Institut für Festkörperforschung Stuttgart (Germany) 1997.
- [36] O. Jepsen, O.K. Andersen, Z. Phys. B. 97 (1995) 35.
- [37] O.K. Andersen, O. Jepsen, Phys. Rev. Lett. 53 (1984) 2571.
- [38] R. Dronskowski, P.E. Blochl, Journal of Physical Chemistry 97 (1993) 8617-8624.
- [39] K. Momma, F. Izumi, (2008) VESTA: a three-dimensional visualization system for electronic and structural analysis.
- [40] Z. Ban, M. Sikirica, Acta Cryst. 18 (1965) 594-599.
- [41] G. Gavaille, N.K. Hansen, R. Welter, B. Malaman, P. Herzig, H.G. Krane, J. Phys.: Condens. Matter 12 (2000) 2667-2679.
- [42] J. Leciejewicz, S. Siek, A. Szytula, J. Less Comm. Mat. 144 (1988) 9-13.
- [43] N. Ni, S. Nandi, A. Kreyssig, A.I. Goldman, E.D. Mun, S.L. Bud'ko, P.C. Canfield, Phys. Rev. B 78 (2008) 014523.
- [44] P.C. Canfield, S.L. Bud'ko, N. Ni, A. Kreyssig, A.I. Goldman, R.J. McQueeney, M.S. Torikachvili, D.N. Argyriou, G. Luke, W. Yu, Physica C 469 (2009) 404-412.
- [45] Y. Qi, L. Wang, Z. Gao, D. Wang, X. Zhang, C. Wang, C. Yao, Y. Ma, New J. Phys. 13 (2011) 033020.
- [46] V.B. Zinth, Dissertation Ludwig-Maximilians-Universität München (2012).
- [47] R.D. Shannon, Acta Crystallogr. Sect. A 32 (1976) 751-767.
- [48] Y. Singh, Y. Lee, S. Nandi, A. Kreyssig, A. Ellern, S. Das, R. Nath, B.N. Harmon, A.I. Goldman, D.C. Johnston, Phys. Rev. B 78 (2008) 104512.
- [49] V.B. Zinth, V. Petricek, M. Dusek, D. Johrendt, Phys. Rev. B 85 (2012) 014109.
- [50] T. Yildirim, Physical Review Letters. 102 (2009) 037003.
- [51] V. Hlukhyy, N. Chumalova, V. Zaremba, T.F. Fässler, Z. Anorg. Allg. Chem. 634 (2007) 1249-1255.
- [52] M. Kohout, F.R. Wagner, Y. Grin, Theor. Chem. Acc. 108 (2002) 150-156.
- [53] V. Hlukhyy, A. Senyshyn, D. Trots, F. T.F., HASYLAB Ann. Rep. 1 (2007) 1021.
- [54] E.A. Leon-Escamilla, J.D. Corbett, J. Solid State Chem. 159 (2001) 149-162.
- [55] H. Watanabe, K. Ito, H. Yamamoto, J. Phys. Soc. Jpn. 18 (1963) 995.
- [56] A. Osawa, T. Murata, Nippon Kinzoku Gakkai Kaiho 4 (1940) 228-242.
- [57] J. Engstroem, T. Johnsson, Acta Chem. Scand. 19 (1965) 1508.
- [58] B. Boren, Ark. Kemi, Mineral. Geol. A 11 (1933) 1-28.
- [59] H.W. Rocktäschel, A. Weiss, Z. Anorg. Allg. Chem. 316 (1962) 231.

Table 1 Crystal Data and structure refinement for CaFe_2Si_2 , $\text{CaFe}_{0.68(6)}\text{Rh}_{1.32(6)}\text{Si}_2$, CaRh_2Si_2 and SrCo_2Si_2 . All data given in this table refer to X-ray single crystal data at $T = 293 \text{ K}$ refined with cell parameters taken from X-ray powder data for ternary compounds.

Empirical formula	CaFe_2Si_2	$\text{CaFe}_{0.68(6)}\text{Rh}_{1.32(6)}\text{Si}_2$	CaRh_2Si_2	SrCo_2Si_2
Formula weight / $\text{g}\cdot\text{mol}^{-1}$	207.96	264.43	302.08	261.66
Space group, Z	$I4/mmm$, 2	$I4/mmm$, 2	$I4/mmm$, 2	$I4/mmm$, 2
Unit cell dimensions / \AA	$a = 3.939(1)$	$a = 4.059(1)$	$a = 4.070(1)$	$a = 3.974(1)$
(powder data; single crystal data for $\text{CaFe}_{0.68(6)}\text{Rh}_{1.32(6)}\text{Si}_2$)	$c = 10.185(1)$	$c = 9.939(1)$	$c = 9.984(1)$	$c = 10.395(2)$
	$V = 158.0(1)$	$V = 163.8(1)$	$V = 165.3(1)$	$V = 164.2(1)$
Calculated density / $\text{g}\cdot\text{cm}^{-3}$	4.372	5.363	6.068	5.293
Absorption coefficient / mm^{-1}	11.254	11.591	11.963	26.607
$F(000)$	200	246	276	240
Crystal size / mm	0.04 x 0.04 x 0.005	0.12 x 0.06 x 0.02	0.05 x 0.04 x 0.01	0.07 x 0.06 x 0.01
θ range / $^\circ$	4.00 to 29.15	4.10 to 29.70	4.08 to 32.79	3.91 to 32.49
Range in hkl	$\pm 5, \pm 5, \pm 13$	$-5 \leq k \leq 3, \pm 5, \pm 13$	$\pm 6, \pm 5, -14 \leq l \leq 15$	$\pm 5, -4 \leq k \leq 5, \pm 14$
Reflections collected	1463	1335	1570	1418
Independent reflections	85 ($R_{\text{int}} = 0.1107$)	90 ($R_{\text{int}} = 0.0368$)	114 ($R_{\text{int}} = 0.0782$)	95 ($R_{\text{int}} = 0.097$)
Reflections with $I \geq 2\sigma(I)$	68 ($R_\sigma = 0.0318$)	89 ($R_\sigma = 0.0115$)	90 ($R_\sigma = 0.0301$)	87 ($R_\sigma = 0.033$)
Data/parameters	68/8	90/10	90/9	87/8
GOF on F^2	1.317	1.763	1.093	1.163
Final R indices [$I \geq 2\sigma(I)$]	$R_1 = 0.0452$	$R_1 = 0.030$	$R_1 = 0.026$	$R_1 = 0.036$
	$wR_2 = 0.103$	$wR_2 = 0.062$	$wR_2 = 0.073$	$wR_2 = 0.090$
R indices (all data)	$R_1 = 0.068$	$R_1 = 0.030$	$R_1 = 0.035$	$R_1 = 0.038$
	$wR_2 = 0.112$	$wR_2 = 0.063$	$wR_2 = 0.075$	$wR_2 = 0.091$
Largest diff. peak and hole / $\text{e}\cdot\text{\AA}^{-3}$	0.926 and -0.850	1.234 and -0.808	3.943 and -2.518	1.526 and -1.320

Table 2 Atomic coordinates and isotropic equivalent displacement parameters $/\text{\AA}^2 \times 10^3$ for CaFe_2Si_2 , $\text{CaFe}_{0.68(6)}\text{Rh}_{1.32(6)}\text{Si}_2$, CaRh_2Si_2 and SrCo_2Si_2 (space group $I4/mmm$, $Z = 2$).

Atom	Wyckoff position	x	y	z	$U_{\text{eq}} / \text{\AA}^2 \times 10^3$
CaFe_2Si_2					
Ca	$2a$	0	0	0	19(1)
Fe	$4d$	0	1/2	1/4	17(1)
Si	$4e$	0	0	0.3746(4)	18(2)
$\text{CaFe}_{0.68(6)}\text{Rh}_{1.32(6)}\text{Si}_2$					
Ca	$2a$	0	0	0	8(1)
Fe/Rh	$4d$	0	1/2	1/4	5(1)
Si	$4e$	0	0	0.3716(4)	7(1)
CaRh_2Si_2					
Ca	$2a$	0	0	0	12(1)
Rh	$4d$	0	1/2	1/4	9(1)
Si	$4e$	0	0	0.3733(4)	12(1)
SrCo_2Si_2					
Sr	$2a$	0	0	0	12(1)
Co	$4d$	0	1/2	1/4	11(1)
Si	$4e$	0	0	0.3606(3)	12(1)

Table 3 Interatomic distances calculated with the lattice parameters taken from X-ray powder data for SrCo_2Si_2 , CaFe_2Si_2 , CaRh_2Si_2 and from single crystal data for $\text{CaFe}_{0.68(6)}\text{Rh}_{1.32(6)}\text{Si}_2$ (space group $I4/mmm$, $Z = 2$) and selected corresponding integrated crystal orbital Hamilton populations (-iCOHPs) values at E_F .

		distance / Å	iCOHP / eV			distance / Å	iCOHP / eV
CaFe₂Si₂							
Ca	-Ca	3.938(1)	-	Si	-Fe	2.343(2)	2.71
	-Fe	3.219(1)	-		-Si	2.555(9)	1.98
	-Si	3.064(2)	0.65	Fe	-Fe	2.785(1)	1.17
CaFe_{0.68(6)}Rh_{1.32(6)}Si₂							
Ca	-Ca	4.059(1)	-	Si	-Fe/Rh	2.362(2)	-
	-	3.208(1)	-		-Si	2.552(6)	-
	Fe/Rh						
	-Si	3.141(2)	-	Fe/Rh	-Fe/Rh	2.870(1)	-
CaRh₂Si₂							
Ca	-Ca	4.069(2)	-	Si	-Rh	2.378(1)	2.68
	-Rh	3.220(1)	-		-Si	2.529(8)	2.10
	-Si	3.143(2)	0.65	Rh	-Rh	2.878(1)	1.02
SrCo₂Si₂							
Sr	-Sr	3.974(1)	-	Si	-Co	2.296(3)	2.80
	-Co	3.271(1)	-		-Si	2.898(5)	0.93
	-Si	3.162(3)	0.66	Co	-Co	2.810(1)	0.94

Table 4 Tetrahedral angles $\alpha / ^\circ$ within the $[T\text{-Si}]$ layer of the title compounds.

Compound	$\alpha (\text{Si-T-Si}) / ^\circ$
CaFe_2Si_2	114.4(2)
$\text{CaFe}_{0.68(6)}\text{Rh}_{1.32(6)}\text{Si}_2$	118.5(8)
CaRh_2Si_2	117.6(3)
SrCo_2Si_2	119.9(2)

Table 5 Lattice parameters, atomic distances and tetrahedral angles (α) of AeT_2Si_2 ($Ae = Ca, Sr, Ba$; $T = Fe, Co, Ni, Cu, Zn, Pd, Ag$) compounds ($I4/mmm$ space group, $Z = 2$).

Compound	$a / \text{\AA}$	$c / \text{\AA}$	$V / \text{\AA}^3$	c/a	$d(T-T) / \text{\AA}$	$d(T-Si) / \text{\AA}$	$d(Si-Si) / \text{\AA}$	$\alpha / ^\circ$	Ref.
CaFe ₂ Si ₂	3.939(1)	10.185(1)	158.0(1)	2.59	2.785(1)	2.343(2)	2.555(9)	114.4(2)	*
CaCo ₂ Si ₂	3.92	9.92	152.1	2.53	2.77	2.29	2.58	117.4	[3]
CaNi ₂ Si ₂	3.99	9.67	153.8	2.43	2.82	2.31	2.49	119.1	[41]
CaCu ₂ Si ₂	4.04	10.0	163.22	2.48	2.86	2.42	2.32	112.9	[23]
CaZn ₂ Si ₂	4.17	10.58	184.2	2.54	2.95	2.55	2.36	109.9	[21]
SrCo ₂ Si ₂	3.974(1)	10.395(2)	164.2(1)	2.62	2.810(1)	2.296(3)	2.898(5)	119.9(2)	*
SrCu ₂ Si ₂	4.20	10.00	176.4	2.48	2.97	2.47	2.42	116.9	[23]
SrZn ₂ Si ₂	4.33	10.35	194.1	-	-	-	-	-	[21] [#]
BaZn ₂ Si ₂	4.50	10.20	206.4	2.27	3.18	2.61	2.43	118.6	[2]
CaRh ₂ Si ₂	4.070(1)	9.984(1)	165.3(1)	2.45	2.878(1)	2.378(1)	2.529(8)	117.6(3)	*
CaPd ₂ Si ₂	4.22	9.77	173.7	2.32	2.98	2.43	2.44	119.9	[20]
SrPd ₂ Si ₂	4.31	9.88	183.5	2.29	3.05	2.48	2.47	120.4	[20]
SrAg ₂ Si ₂	4.38	10.48	201.1	2.39	3.10	2.63	2.33	112.7	[22]

* this work

[#] Cell parameters from X-ray powder data, no single crystal data measured to confirm ThCr₂Si₂ type structure.

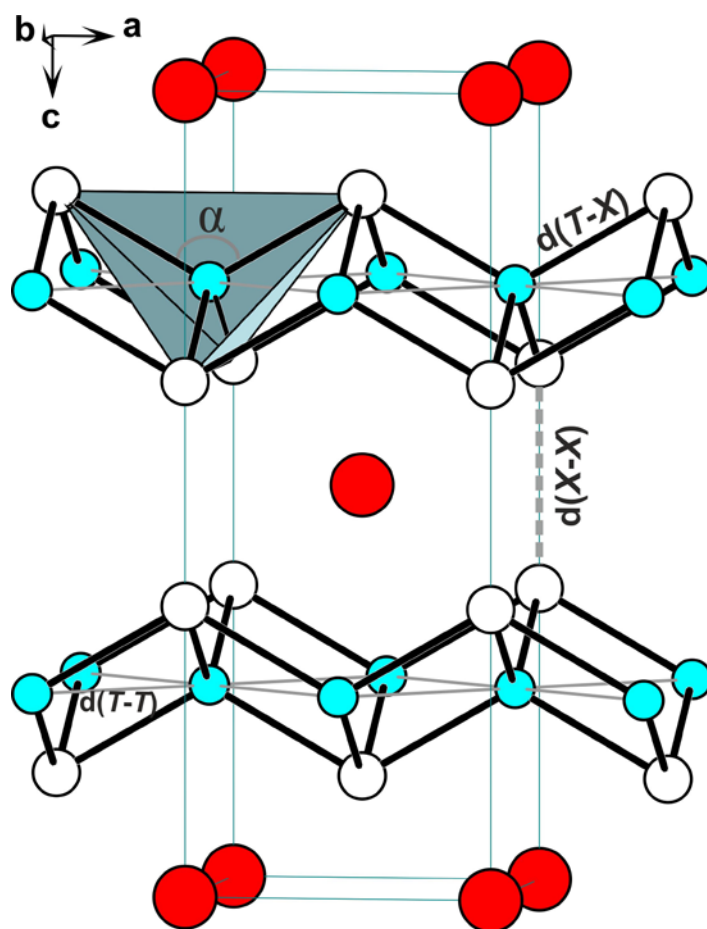


Figure 1. Structure of SrCo_2Si_2 (Sr - red, Co - blue, Si - white) displayed as a model including selected structural parameters for the ThCr_2Si_2 -type structure.

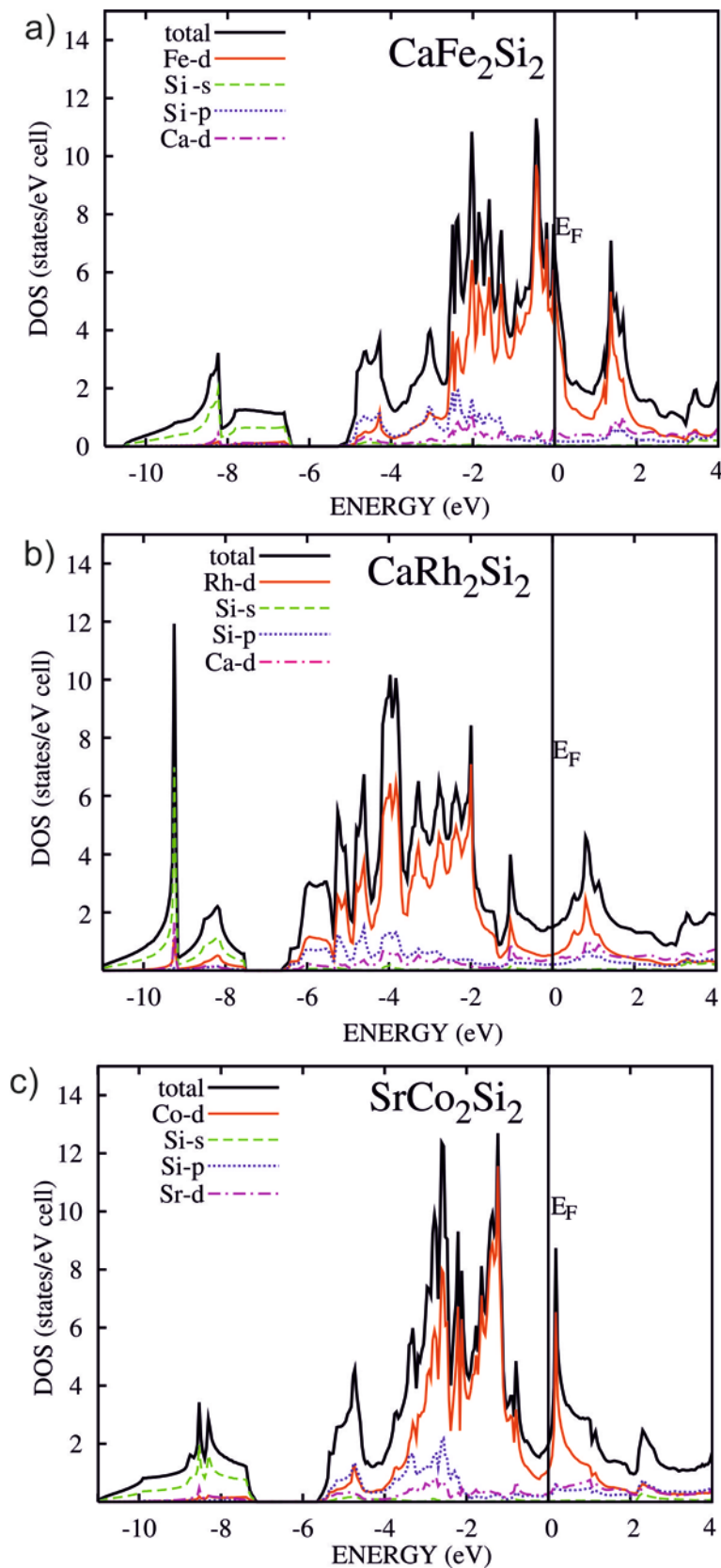


Figure 2. DOS and projected DOS calculated for a) CaFe_2Si_2 , a) CaRh_2Si_2 and c) SrCo_2Si_2 . The energy zero is taken at the Fermi level (for comparison the DOS for CaCo_2Si_2 is presented in Supporting Information, Figure S8).

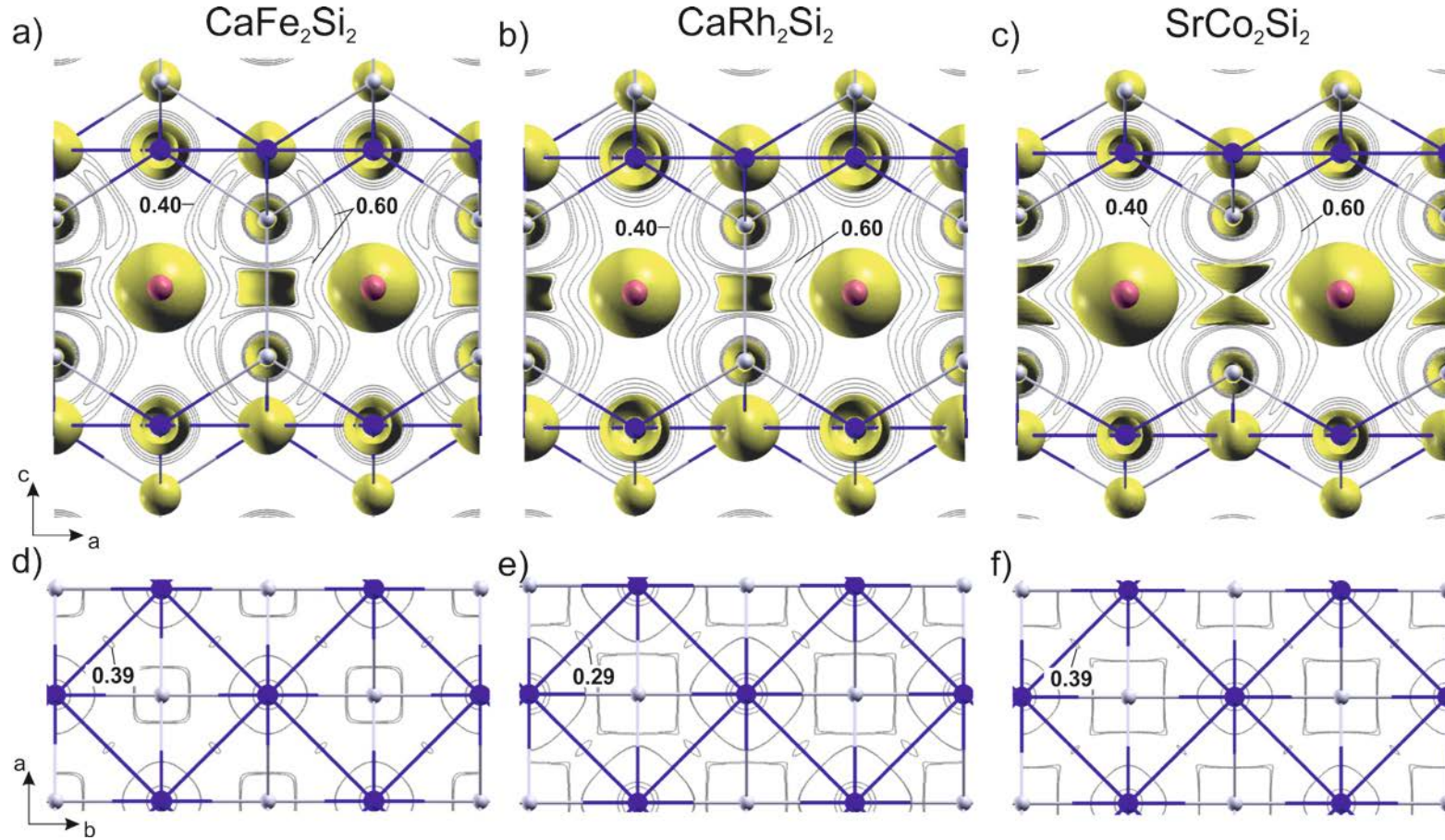


Figure 3. Topology of the ELF for CaFe_2Si_2 , CaRh_2Si_2 and SrCo_2Si_2 calculated from the all-electron density (TB-LMTO-ASA). A 3D ELF plot with isosurface at $\eta = 0.72$ and contour line diagrams of the ELF in the ac plane present the Si-Si bonding in CaFe_2Si_2 (a), CaRh_2Si_2 (b), and lone electron pairs at the Si atoms in SrCo_2Si_2 (c). Contour line diagrams of the ELF in the ab plane of CaFe_2Si_2 (d), CaRh_2Si_2 (e), and SrCo_2Si_2 (f) emphasise weak T - T interactions. For the clarity only the regions of $\eta = 0.39 - 0.40$, $\eta = 0.285 - 0.29$ and $\eta = 0.39 - 0.40$ for CaFe_2Si_2 , CaRh_2Si_2 and SrCo_2Si_2 , respectively, were chosen.

Supporting Information

Synthesis and structure of SrCo_2Si_2 and CaRh_2Si_2 - isoelectronic variants of the parent superconductors AeFe_2As_2 and study of the influence of the valence electron count in $\text{CaFe}_{2-x}\text{Rh}_x\text{Si}_2$

Viktor Hlukhyy, Andrea V. Hoffmann, Thomas F. Fässler

Table S1 Lattice parameters, atomic distances and tetrahedral angles (α) of AeT_2Ge_2 ($Ae = \text{Ca-Ba}$, $T = \text{Mn-Zn}$) compounds (ThCr₂Si₂-type structure, $I4/mmm$, $Z = 2$).

Compound	a / Å	c / Å	V / Å ³	c/a	$d(T-T)$ / Å	$d(T-Ge)$ / Å	$d(Ge-Ge)$ / Å	α / °	Ref.
CaMn ₂ Ge ₂	4.17	10.88	189.2	2.61	2.95	2.53	2.59	111.3	[17]
CaCo ₂ Ge ₂	4.00	10.33	165.3	2.58	2.83	2.36	2.67	116.0	[17]
CaNi ₂ Ge ₂	3.99	9.67	153.8	2.43	2.82	2.31	2.49	119.1	[41]
CaCu ₂ Ge ₂	4.14	10.23	175.3	2.47	2.93	2.45	2.48	114.9	[23]
CaZn ₂ Ge ₂	4.21	10.85	192.3	2.58	2.98	2.57	2.47	109.9	[23]
SrMn ₂ Ge ₂	4.30	10.91	201.7	2.54	3.04	2.58	2.62	113.2	[17]
SrCo ₂ Ge ₂	4.08	10.65	177.3	2.61	2.89	2.37	2.90	118.5	[17]
SrNi ₂ Ge ₂	4.17	10.25	178.2	2.46	2.95	2.38	2.83	122.3	[17]
SrCu ₂ Ge ₂	4.28	10.31	188.9	2.41	3.03	2.47	2.70	120.3	[17]
SrZn ₂ Ge ₂	4.37	10.61	202.6	2.43	3.09	2.60	2.50	114.7	[17]
BaMn ₂ Ge ₂	4.47	10.99	219.6	2.46	3.16	2.62	2.75	116.8	[17]
BaCo ₂ Ge ₂	4.09	11.78	196.6	2.88	2.89	2.35	3.55	120.4	[3]
BaNi ₂ Ge ₂	4.27	11.25	204.9	2.64	3.02	2.35	3.64	130.0	[53]

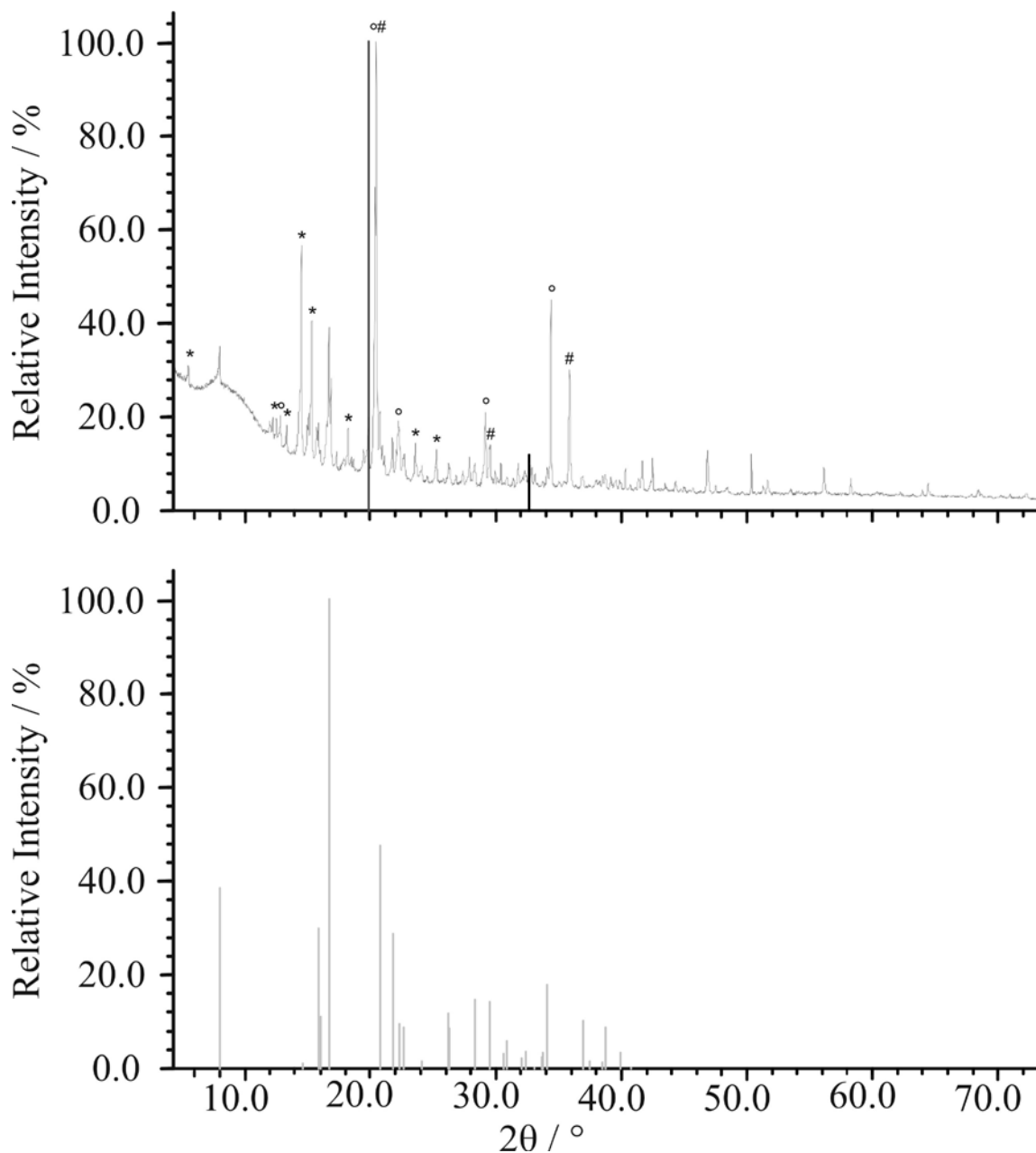


Figure S1. X-ray powder diffraction pattern of CaFe_2Si_2 sample. Theoretical calculated pattern of CaFe_2Si_2 with ThCr_2Si_2 -type structure (light gray lines) indicated in the diffractogram. The reflexes marked with the dark line at 19.8° and 33.65° belong to cubic diamond which was used as an internal standard. Reflexes marked with * belong to Ca_5Si_3 [54], reflexes marked with $^\circ$ belong to FeSi [55] and reflexes marked with # belong to Fe_3Si [56]. (Mo-MythenK-PSD)

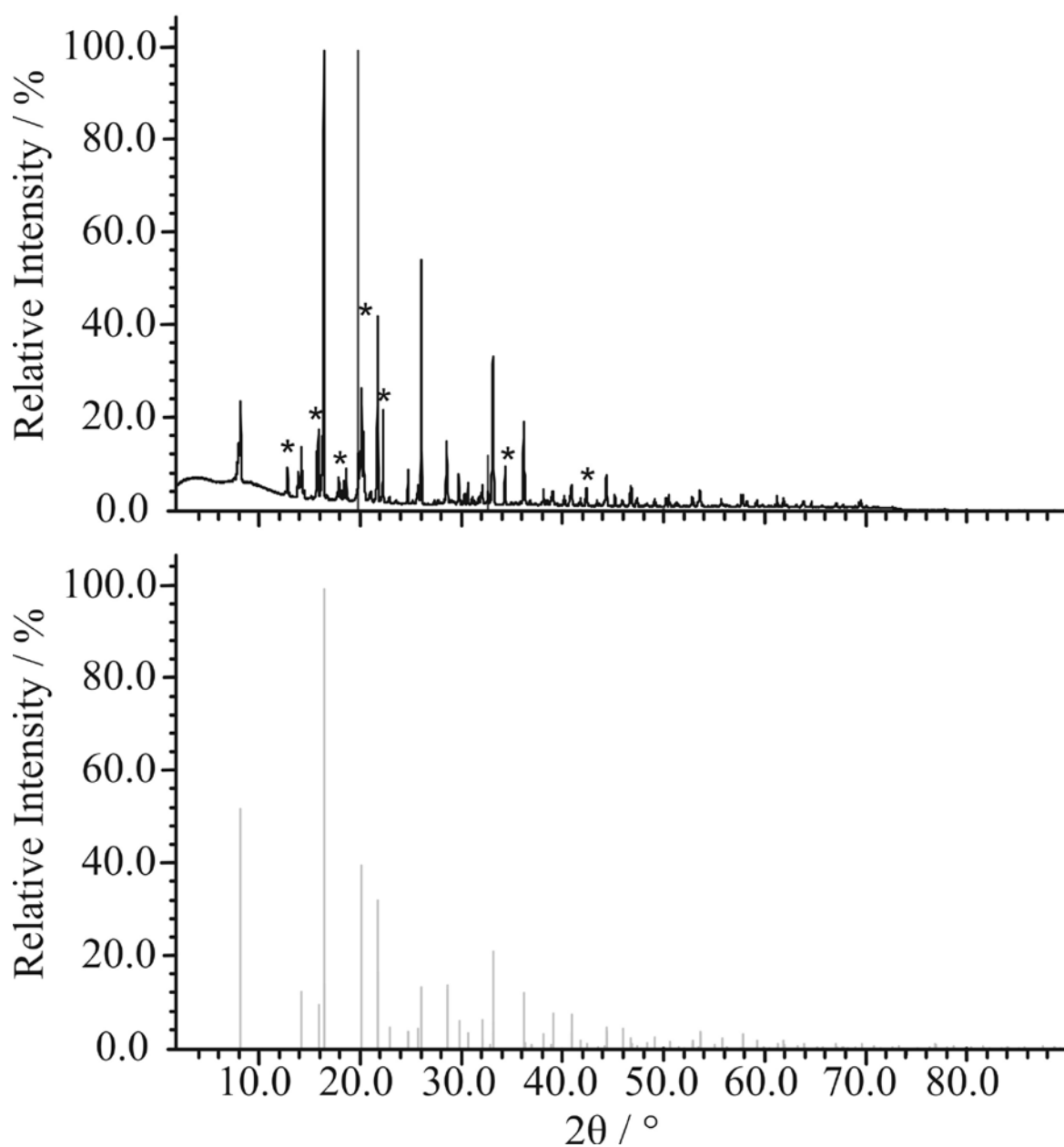


Figure S2. X-ray powder diffraction pattern of $\text{CaFe}_{0.66(3)}\text{Rh}_{1.34(3)}\text{Si}_2$ sample. Theoretically calculated pattern of $\text{CaFe}_{0.66(3)}\text{Rh}_{1.34(3)}\text{Si}_2$ with ThCr_2Si_2 -type structure (light gray lines) indicated in the diffractogram. The reflex marked with the dark line at 19.8° and 33.65° belong to cubic diamond which was used as an internal standard. Reflexes marked with * belong to FeSi [55]. (Mo-MythenK-PSD)

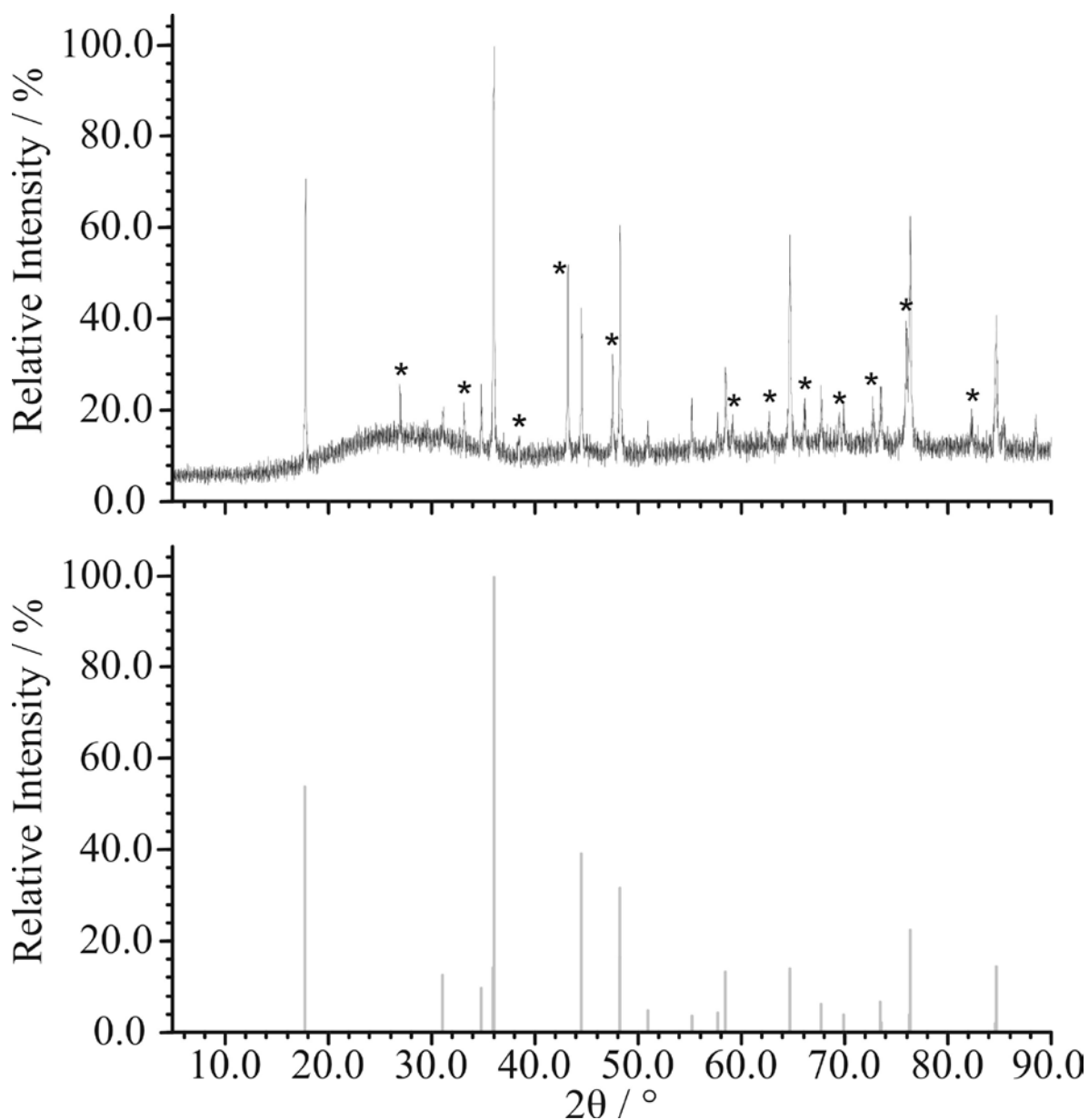


Figure S3. X-ray powder diffraction pattern of CaRh_2Si_2 sample. Theoretical calculated pattern of CaRh_2Si_2 with ThCr_2Si_2 -type structure (light gray lines) indicated in the diffractogram. Reflexes marked with * belong to RhSi [57]. (L-PSD)

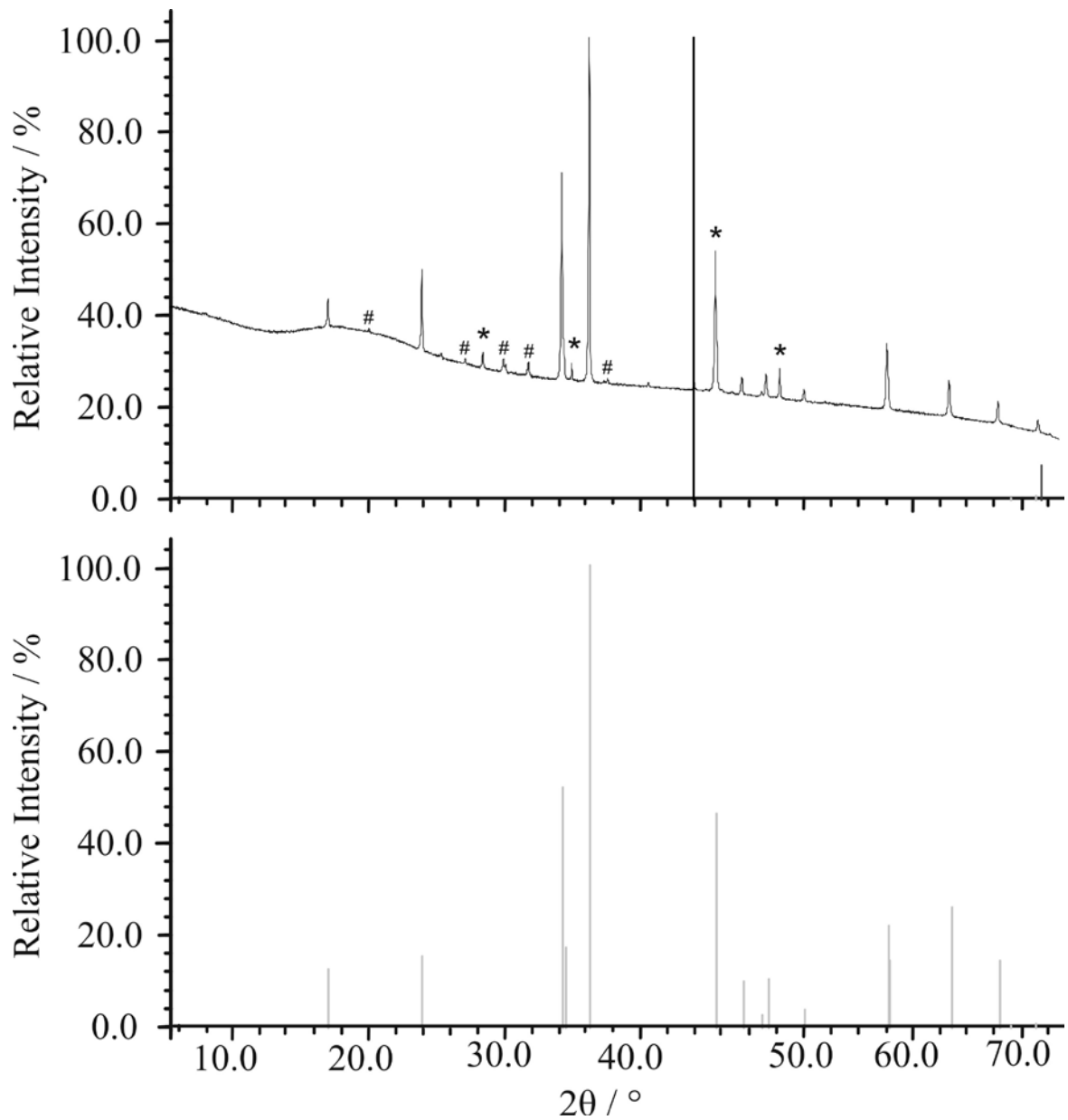


Figure S4. X-ray powder diffraction pattern of SrCo_2Si_2 sample made with the resistance furnace. Theoretically calculated pattern of SrCo_2Si_2 with ThCr_2Si_2 -type structure (light gray lines) indicated in the diffractogram. Reflexes marked with * belong to CoSi [58] and reflexes marked with # belong to SrSi [59]. (L-PSD)

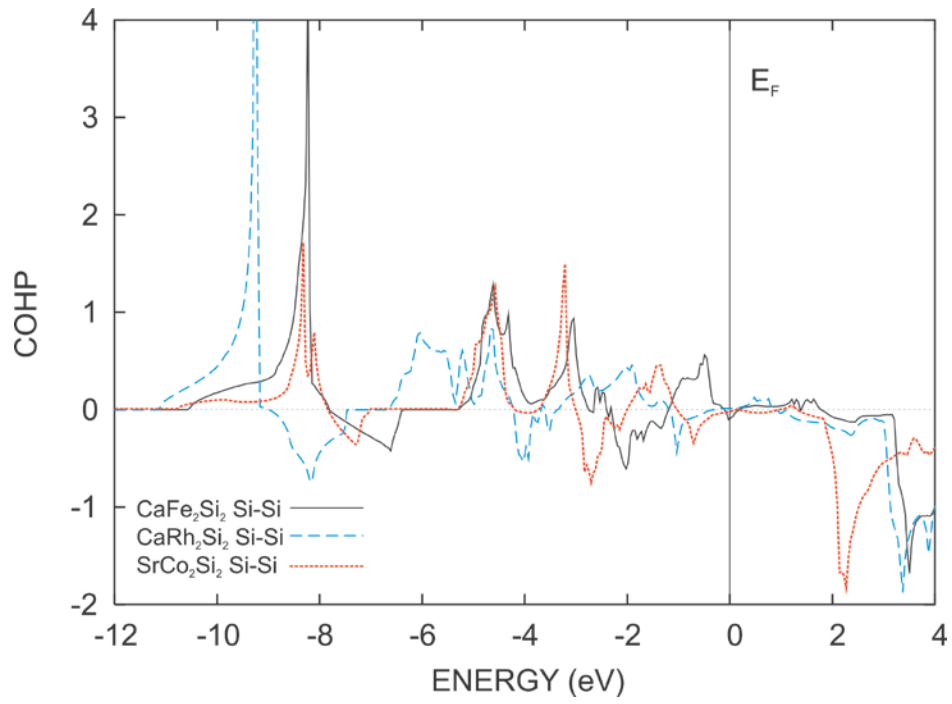


Figure S5. Crystal orbital Hamiltonian populations (COHP) curves for the Si-Si bonds in CaFe_2Si_2 , CaRh_2Si_2 and SrCo_2Si_2 .

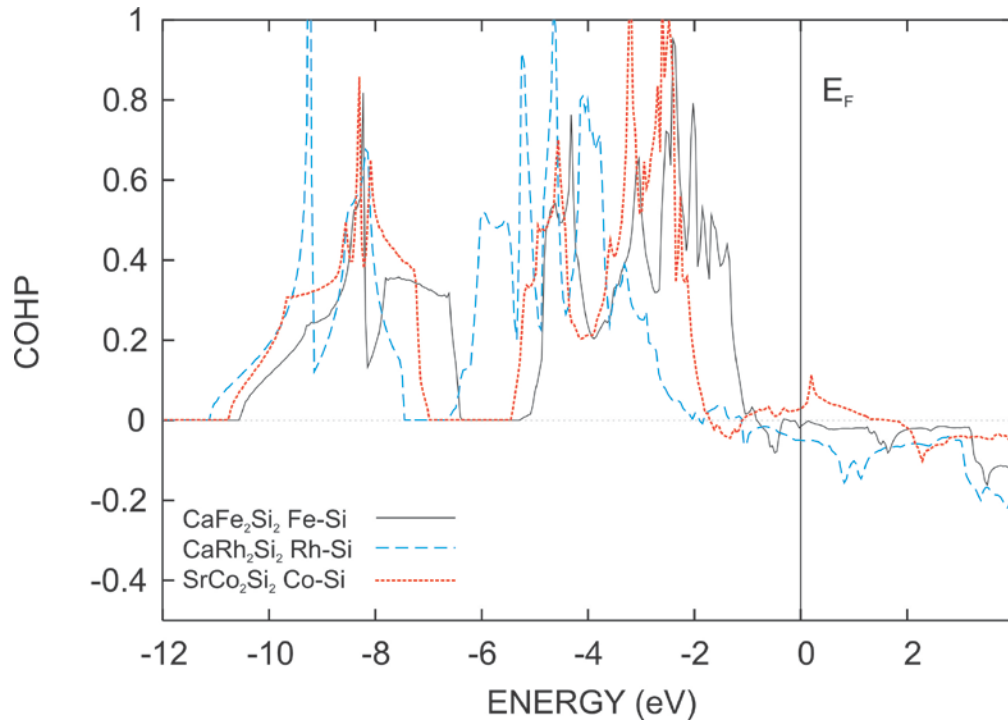


Figure S6. Crystal orbital Hamiltonian populations (COHP) curves for the T -Si bonds in CaFe_2Si_2 , CaRh_2Si_2 and SrCo_2Si_2 .

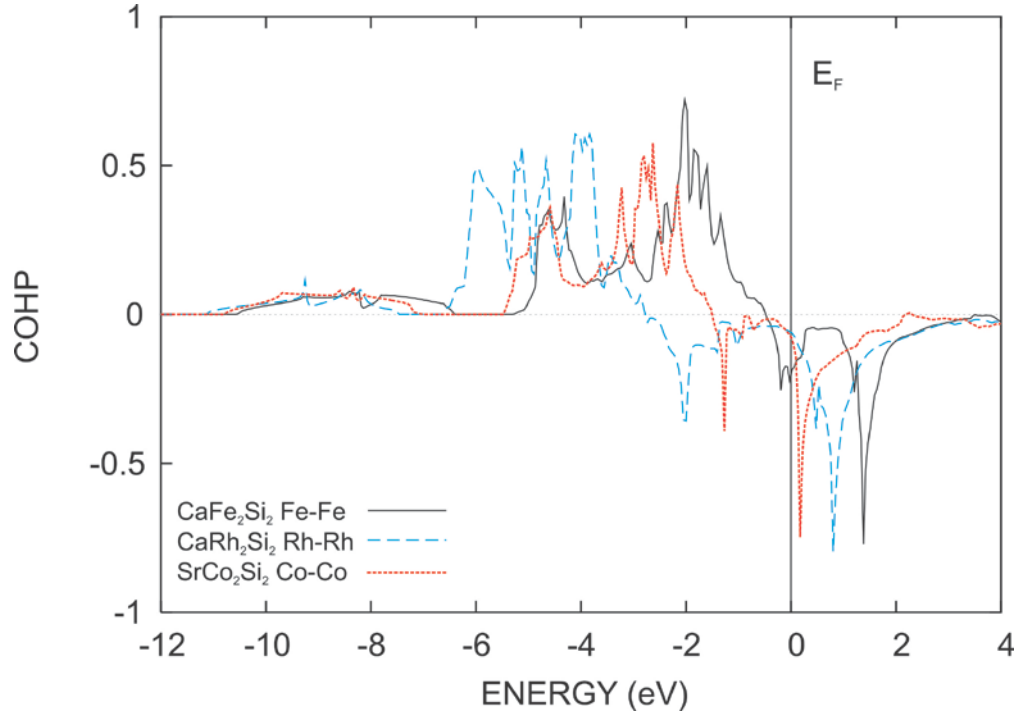


Figure S7. Crystal orbital Hamiltonian populations (COHP) curves for the T - T bonds in CaFe_2Si_2 , CaRh_2Si_2 and SrCo_2Si_2 .

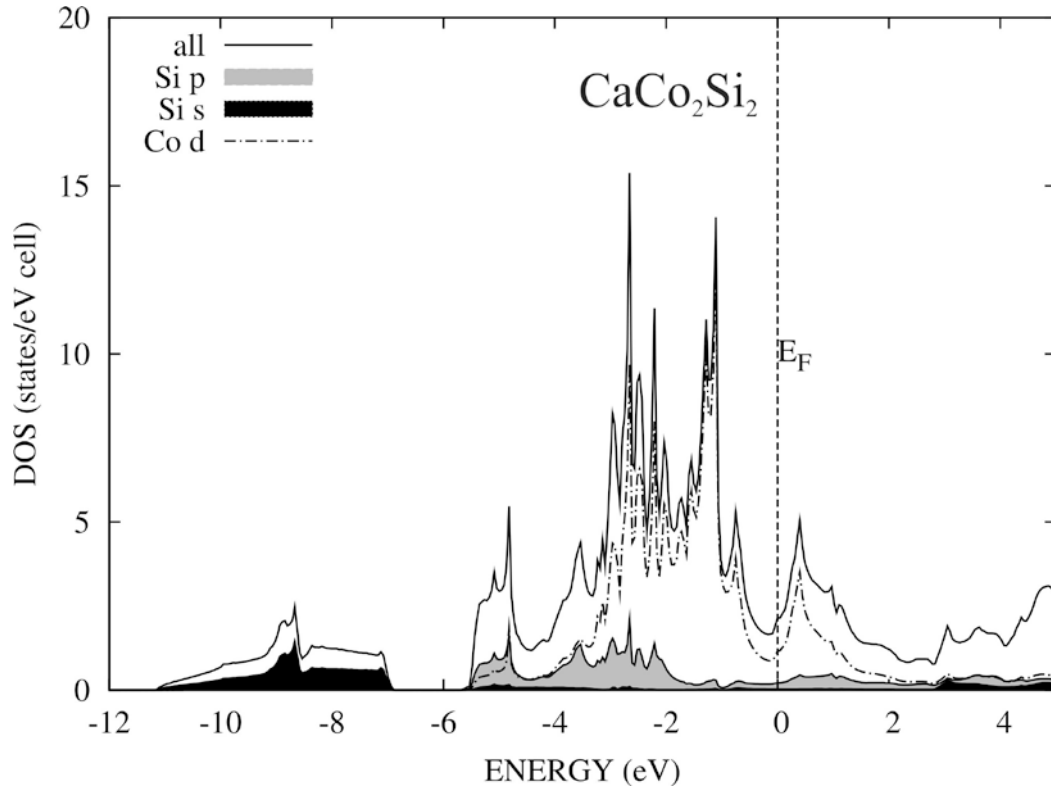


Figure S8. Total DOS and partial DOS calculated for CaCo_2Si_2 . Taken from [3].

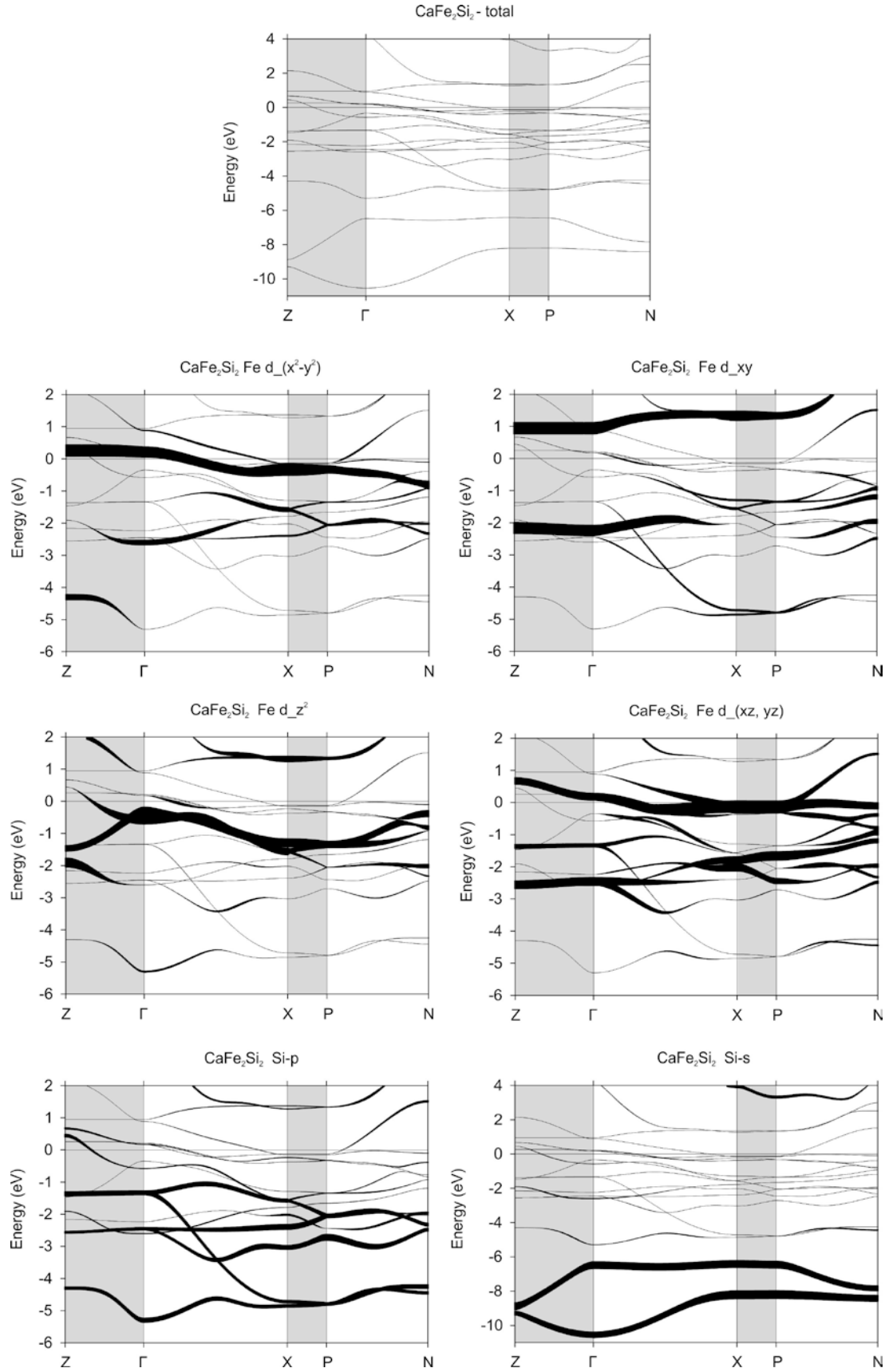


Figure S9. Band structure for CaFe_2Si_2 in the range from -6 eV to 2 eV including fatbands for Fe- $d_{x^2-y^2}$, d_{xy} , d_{z^2} , $d_{xz,yz}$, Si- p, s orbitals.

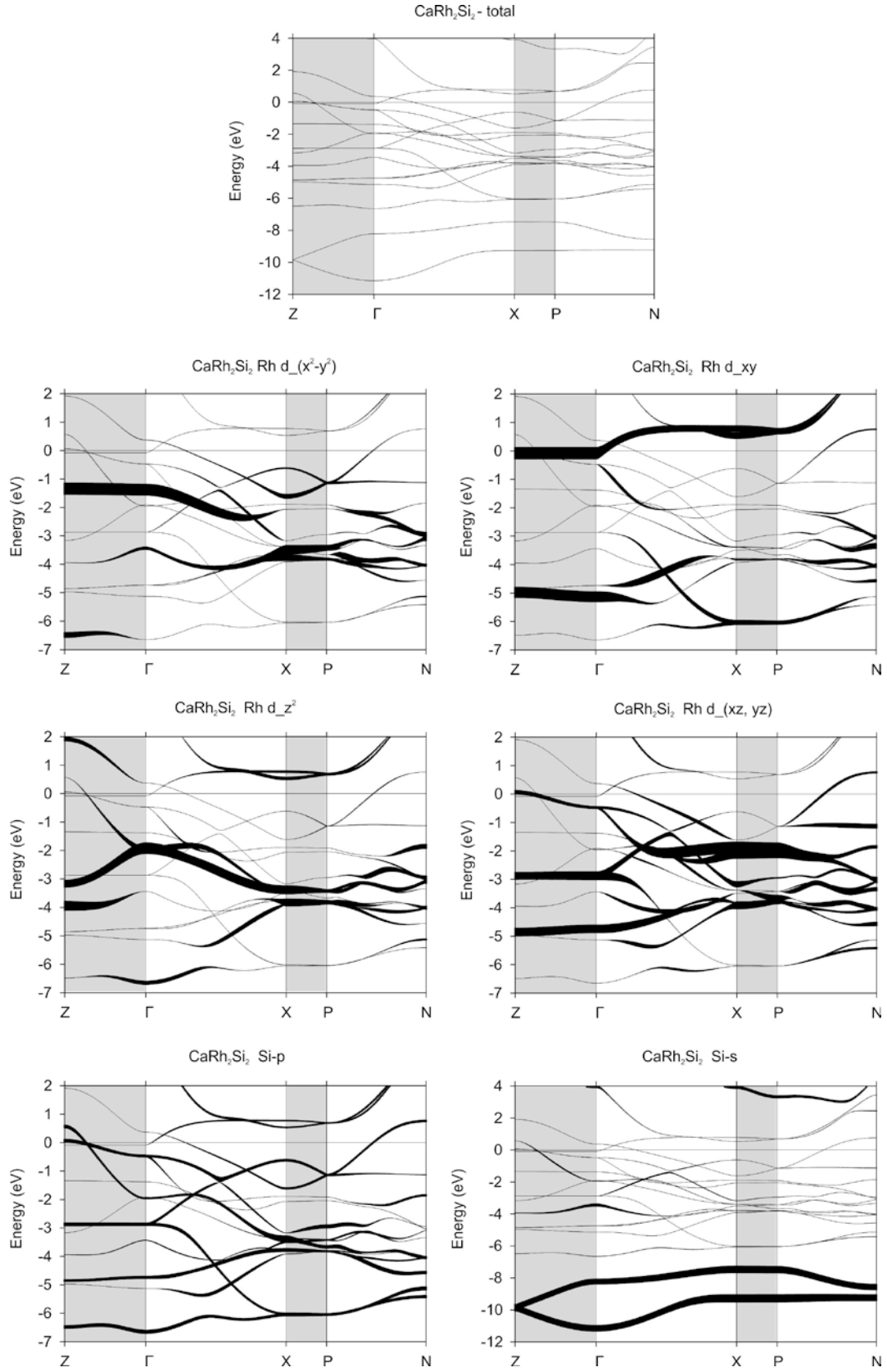


Figure S10. Band structure for CaRh_2Si_2 in the range from -6 eV to 2 eV including fatbands for Rh- $d_{x^2-y^2}$, d_{xy} , d_{z^2} , $d_{xz,yz}$, Si- p, s orbitals.

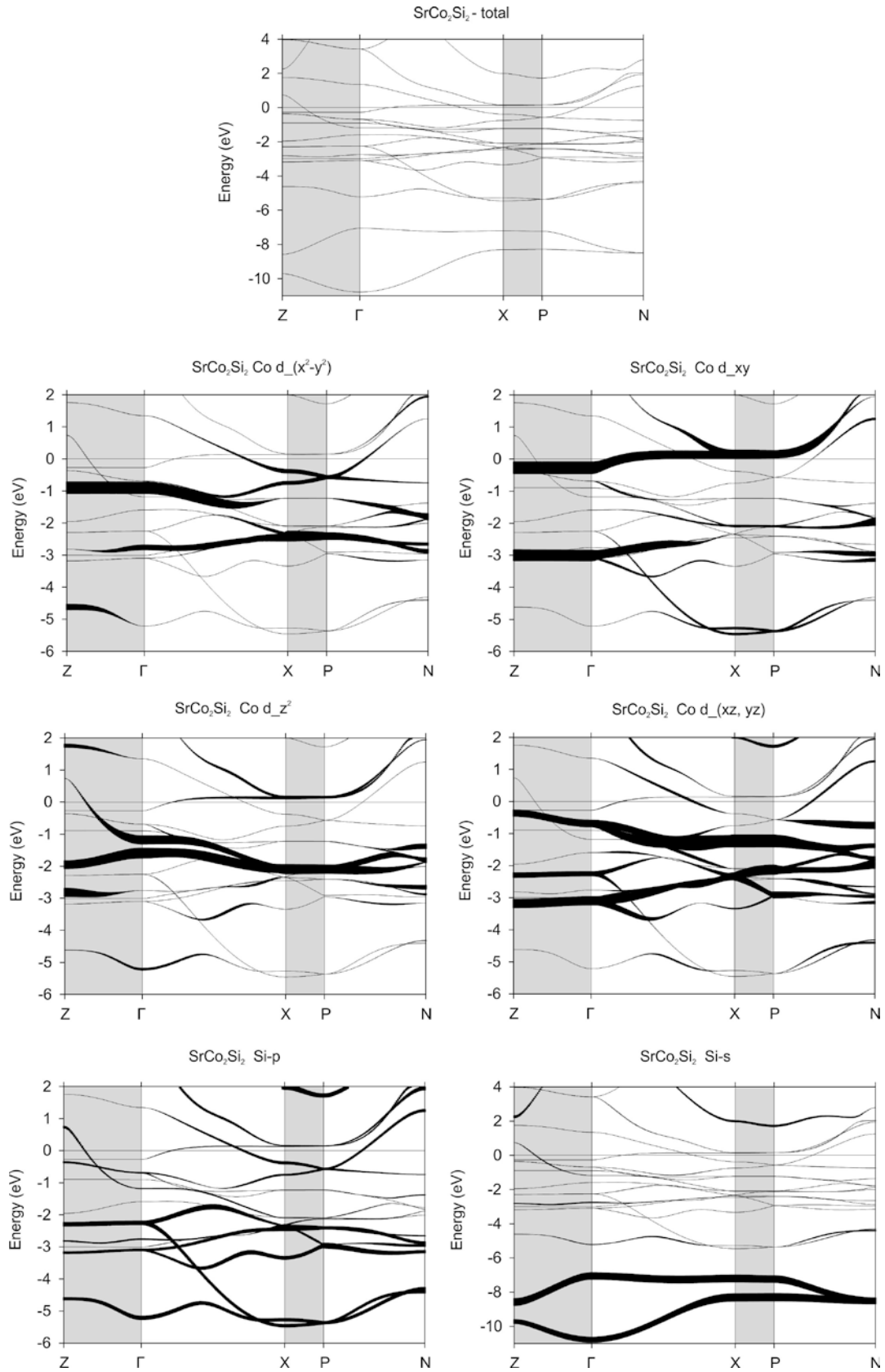


Figure S11. Band structure for SrCo_2Si_2 in the range from -6 eV to 2 eV including fatbands for Co- $d_{x^2-y^2}$, d_{xy} , d_{z^2} , $d_{xz,yz}$, Si- p, s orbitals.